

4-point correlators in finite-temperature AdS/CFT: jet quenching correlations

Peter Arnold and Diana Vaman

*Department of Physics, University of Virginia,
Box 400714, Charlottesville, Virginia 22904, USA*

(Dated: October 6, 2018)

Abstract

There has been recent progress on computing real-time equilibrium 3-point functions in finite-temperature strongly-coupled $\mathcal{N}=4$ super Yang-Mills (SYM). In this paper, we show an example of how to carry out a similar analysis for a 4-point function. We look at the stopping of high-energy “jets” in such strongly-coupled plasmas and study the question of whether, on an event-by-event basis, each jet deposits its net charge over a narrow ($\sim 1/T$) or wide ($\gg 1/T$) spatial region. We relate this question to the calculation of a 4-point equilibrium correlator.

I. INTRODUCTION

Real-time, equilibrium, retarded Green functions are important to the study of relaxation in finite-temperature field theory. Through the fluctuation-dissipation theorem, they are directly related to the dynamics of how small deviations from equilibrium relax. In the context of strongly-coupled gauge-theory plasmas with gauge-gravity duality, 2-point retarded Green functions have been used to extract viscosity and other hydrodynamic transport coefficients [1, 2]. 3-point retarded Green functions have been used to (i) extract the stopping distance for certain types of high-momentum “jets” created in the plasma [3–5], and (ii) reproduce earlier results for second-order hydrodynamic coefficients [6, 7] and find the first correction to the large-coupling limits for such coefficients [7]. Finding useful analytic expressions for generic finite-temperature Green functions can be a great challenge, but problems of interest are often limiting cases where the Green functions simplify. For instance, hydrodynamic transport coefficients only depend on the low-momentum limit of the 2-point (or 3-point) function, whereas the 3-point function relevant for the jet problem is one where two of the three momenta are very high and the other is low [3]. In this paper, we will push the analysis of finite-temperature Green functions in such theories one point higher: we will discuss a problem, related to jet stopping, that requires the analysis of a 4-point function. In this application, the four momenta involved will all be either high or low compared to the temperature, which will make the analysis tractable.

Here is the problem we study. We will loosely refer to spatially localized, high-momentum excitations of the plasma as “jets.” Formally, one way to create such jets is to briefly turn on localized, high-momentum source terms in the field theory. In our earlier work [3],¹ we tracked the progress of the resulting jet by measuring the subsequent evolution $\langle j^0(x) \rangle$ of the density j^0 of a conserved charge carried by the jet. We found that the jet’s charge was deposited along the jet’s trajectory according to a distribution depicted in fig. 1. The charge subsequently diffuses hydrodynamically. In fig. 1, L is the space-time size of the localized source that we used to create the jet. Computing $\langle j^0(x) \rangle$, however, only gives us the *averaged* behavior of a jet. From this result alone, one does not know what happens on an event-by-event basis. Does each jet (i) deposit over a wide range of distances? Or, in contrast, does each jet (ii) stop and deposit its conserved charges in a small localized region, with fig. 1 representing a probability distribution for how far the jet travels? Later work [4], which provides a simple way to reproduce fig. 1 in terms of the trajectories of classical 5-dimensional particles in AdS₅-Schwarzschild, supports the second interpretation. It should be possible to verify this interpretation by examining correlations $\langle j^0(x) j^0(y) \rangle$ of the charge density in the presence of the source. If charge deposition is indeed localized for each individual event, then there should be no significant correlation between charge deposition at significantly different distances.

As we shall review, the evolution $\langle j^0(x) \rangle$ of the charge density in the presence of the source is related to an equilibrium, retarded 3-point function between (i) the measured charge density and (ii) source operators associated with the creation of the jet. The corresponding Witten diagram in the gravity dual is depicted in fig. 2a. Correlations such as $\langle j^0(x) j^0(y) \rangle$ will correspond to equilibrium 4-point functions, and fig. 2b gives an example of a corresponding Witten diagram.² Our goal in this paper is to analyze such diagrams.

¹ See ref. [5] for a very short, breezy, and detail-free overview of ref. [3],

² For a recent discussion of 4-point current correlators at *zero* temperature, see ref. [8].

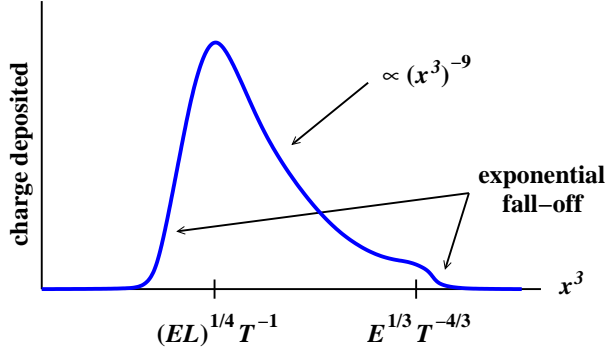


FIG. 1: A qualitative picture of the average deposition of charge as a function of x^3 for jets created by the source described in Sec. II B and in ref. [3].

We will see later that, for the question of interest here, the internal line of fig. 2b is a bulk-to-bulk propagator with both bulk points located near the horizon. There is a relatively simple formula for the near-horizon bulk-to-bulk propagator, which will be a key feature in making the analysis tractable.

At the end of our analysis, we will see that there is indeed no significant correlation between charge deposition at positions separated by $\gg 1/T$.

In the next section, we discuss exactly what field theory correlator we need to measure in order to look for correlations between jet charge deposition at different locations. In particular, we will discuss how to define a correlator $\langle \hat{\Theta}(x) \hat{\Theta}(y) \rangle_{\text{jet}}$ of “charge deposition” $\hat{\Theta}(x)$ and what refinements are necessary to only capture the physics that we want. Section III is devoted to a discussion of exactly what type of equilibrium 4-point correlator we need in order to evaluate $\langle \hat{\Theta}(x) \hat{\Theta}(y) \rangle_{\text{jet}}$ and its relatives and the corresponding Witten diagrams. We start with a review of (r,a) notation for Schwinger-Keldysh formalism. Then we show that we need a 4-point correlator known as G_{arr} , and we argue that there is only a single Witten diagram (fig. 2b with certain specifications for the causality properties of the propagators) relevant to the jet deposition question posed in this introduction. In preparation for the calculation of that diagram, section IV examines the equilibrium bulk-to-bulk correlator G_{rr} in the gravity dual, which will be needed for the internal line in fig. 2b. We show how it can be related to standard bulk-to-boundary propagators. It turns out that only the case where both bulk points are very close to the horizon will be relevant, and we show that the propagators all have a simple structure in that limit. With all these preparations in hand, in section V we finally calculate the diagram and show that charge deposition is localized on an event-by-event basis. Various matters are left for appendices, and in particular Appendix B relates our discussion of bulk-to-bulk G_{rr} to a recent discussion by Caron-Huot, Chesler, and Teaney [10].

II. GENERAL SETUP

A. Notation

We will use capital roman letters to denote 5-dimensional space-time coordinates (e.g. $I, J = 0, 1, 2, 3, 5$) and lower-case Greek letters for 4-dimensional space-time coordinates

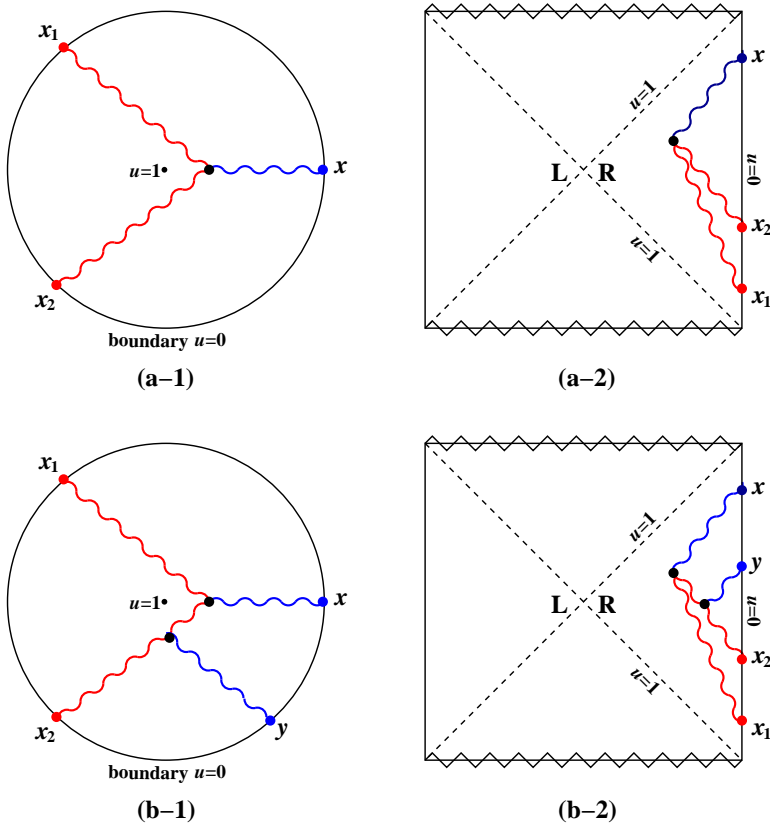


FIG. 2: Examples of Witten diagrams in AdS₅-Schwarzschild space for (a) a 3-point correlation contributing to $\langle j^0(x) \rangle$ in the presence of source operators at x_1 and x_2 , and (b) a 4-point correlation similarly contributing to $\langle j^0(x) j^0(y) \rangle$. In both cases, the first diagram depicts traditional Witten diagrams drawn in imaginary time, with the boundary ($u=0$) represented as a circle. The second diagram depicts the same diagram in real time superposed atop a Penrose diagram of AdS₅-Schwarzschild. For the type of correlators that we will examine in this paper, the bulk vertices in the latter case are confined by causality to the right-hand quadrant. Red lines indicate propagators that have large 4-momenta in our calculation (coming from the source) if one transforms to 4-momentum space, and blue lines (associated with measuring hydrodynamic response of charge densities) have low 4-momenta. We have used artistic license when drawing the boundary of the Penrose diagram with all four sides straight [9].

(e.g. $\mu, \nu = 0, 1, 2, 3$).

Throughout this paper, we generally refer to the fifth dimension of AdS₅ as u , where the boundary is at $u = 0$ and the bulk has $u > 0$. Much of the discussion in the paper will be general but, when we get down to some specifics later on, we will choose u with AdS₅-Schwarzschild metric

$$ds^2 = \frac{R^2}{4} \left[\frac{(2\pi T)^2}{u} (-f dt^2 + d\mathbf{x}^2) + \frac{1}{u^2 f} du^2 \right], \quad (2.1)$$

where R is the radius of AdS space, T is the temperature,

$$f \equiv 1 - u^2, \quad (2.2)$$

and the horizon is at $u = 1$. At that time, we will also work in units where $2\pi T = 1$.

For 4-vectors V^μ , we define light-cone coordinates by

$$V^\pm \equiv V^3 \pm V^0, \quad V_\pm \equiv \frac{1}{2}V^\mp = \frac{1}{2}(V^3 \mp V^0). \quad (2.3)$$

When writing integrals over 4-momenta, we will use the shorthand notation

$$\int_Q \cdots \equiv \int \frac{d^4Q}{(2\pi)^4} \cdots. \quad (2.4)$$

B. The Source

One could study this problem by creating a “jet” with most any localized high-energy source and then tracking any conserved charge density. The calculation is easier with some choices than others, and here we will follow ref. [3] and study the propagation of R charge density, using a source that creates R charge.

To later motivate our calculation of jet charge-charge correlations, it will be convenient to discuss sources that create jets with R charge $\gg 1$. On the other hand, it is also convenient to keep the detailed structure of the calculations here as close as possible to our previous calculations in ref. [3], where the source created jets carrying a single unit of R charge. As a compromise, in the main text we will use the single-charge source of ref. [3], described below, when writing down specific formulas involving the source. But little depends on this, and in Appendix A, we discuss how the formulas generalize to cases where the R charge of the jet is large compared to 1.

So, following ref. [3], we modify the 4-dimensional field theory Lagrangian by

$$\mathcal{L} \rightarrow \mathcal{L} + j_\mu^a A_{\text{cl}}^{a\mu}, \quad (2.5a)$$

where j_μ^a are the SU(4) R-charge currents of the theory and A_{cl} is a classical external source. We choose the external source to have the form of (i) a high-energy plane wave $e^{i\bar{k}\cdot x}$ times (ii) a smooth, slowly varying, real-valued envelope function $\Lambda_L(x)$ localizing the source to a space-time region of size L . Exactly as in ref. [3], we take

$$A_{\text{cl}}^\mu(x) = \bar{\varepsilon}^\mu \mathcal{N}_A \left[\frac{\tau^+}{2} e^{i\bar{k}\cdot x} + \text{h.c.} \right] \Lambda_L(x), \quad (2.5b)$$

where

$$\bar{k}^\mu = (E, 0, 0, E) \quad (2.6)$$

is a very large light-like 4-momentum with frequency $E \gg T$; \mathcal{N}_A is an arbitrarily small source amplitude; $\bar{\varepsilon}$ is a transverse linear polarization, such as

$$\bar{\varepsilon}^\mu = (0, 1, 0, 0); \quad (2.7)$$

and τ^i are Pauli matrices for any SU(2) subgroup of the SU(4) R-symmetry, with

$$\tau^\pm = \tau^1 \pm i\tau^2. \quad (2.8)$$

A simple example of an appropriate envelope function would be

$$\Lambda_L(x) = e^{-\frac{1}{2}(x_0/L)^2} e^{-\frac{1}{2}(x_3/L)^2}. \quad (2.9)$$

L should be chosen large compared to $1/E$, so that the momentum components in the source are all close to (2.6), but small compared to the large stopping distance that we wish to study. The creation of R charge by the source (2.5) is analogous to a decay $W^+ \rightarrow u\bar{d}$ of a very high momentum W boson creating a localized excitation with isospin in a standard-model quark-gluon plasma.

C. The Measurement: Previous Work

In previous work [3], we measured the late-time behavior of

$$\langle j^{(3)0}(x) \rangle_{A_{\text{cl}}} \quad (2.10)$$

for a system that started in thermal equilibrium. The superscript “(3)” indicates the R current associated with $\tau^3/2$ in the SU(2) subgroup referenced by (2.8). The subscript “ A_{cl} ” indicates that the expectation is taken with the source term (2.5a) present in the Lagrangian. As reviewed in ref. [3], expanding to leading order in the small-amplitude source gives

$$\langle j^{(3)\mu}(x) \rangle_{A_{\text{cl}}} = \frac{1}{2} \int d^4x_1 d^4x_2 G_{\text{aar}}^{(ab3)\alpha\beta\mu}(x_1, x_2; x) A_{\alpha, \text{cl}}^a(x_1) A_{\beta, \text{cl}}^b(x_2), \quad (2.11)$$

or equivalently

$$\langle j^{(3)\mu}(x) \rangle_{A_{\text{cl}}} = \frac{1}{2} \int_{Q_1 Q_2 Q} G_{\text{aar}}^{(ab3)\alpha\beta\mu}(Q_1, Q_2; Q) A_{\alpha, \text{cl}}^{a*}(Q_1) A_{\beta, \text{cl}}^{b*}(Q_2) e^{iQ \cdot x} (2\pi)^4 \delta^{(4)}(Q_1 + Q_2 + Q), \quad (2.12)$$

where G_{aar} is the retarded, equilibrium 3-point Green function associated with source operators $j \cdot A_{\text{cl}}$ at x_1 and x_2 and the measurement operator $j^{(3)\mu}$ at x .

In this paper, we will use (r,a) notation to indicate different orderings of operators in n -point thermal Green functions. We review and summarize this notation (and fix our normalization conventions) in section III A, but for the moment it’s enough to remark that $G_{\text{aa}\dots\text{ar}}(x_1, x_2, \dots, x_{n-1}; x)$ denotes an n -point retarded Green function where x is the measurement point and x_1, \dots, x_{n-1} are source points.

After a high energy jet stops and thermalizes in the plasma, its charge density diffuses out from the place where the jet stopped. What we most directly want to know is where the charge density was deposited [3, 11]. If locally thermalized charge is deposited with density $\hat{\Theta}(x)$ in the plasma, the late time evolution of the charge will be given by the diffusion equation

$$(\partial_t - D\nabla^2) j^0(x) = \hat{\Theta}(x), \quad (2.13)$$

where [12]

$$D = \frac{1}{2\pi T} \quad (2.14)$$

is the R-charge diffusion constant. We can turn (2.13) around into an operator definition of the charge deposition:³

$$\hat{\Theta}(x) \equiv (\partial_t - D\nabla^2) j^0(x). \quad (2.15)$$

³ The $\bar{Q}\Theta(x)$ of ref. [3] is $\langle \hat{\Theta}(x) \rangle_{A_{\text{cl}}}$ in our notation here.

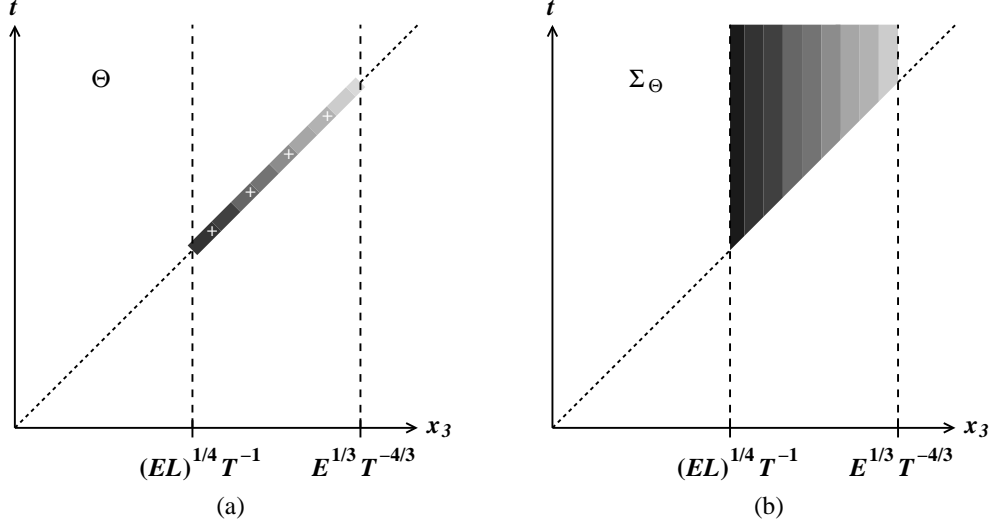


FIG. 3: A cartoon of the space-time distribution of (a) $\langle \hat{\Theta}(x) \rangle$ and (b) $\langle \hat{\Sigma}_\Theta(x) \rangle$ in the region of x^3 where there is net charge deposition. (See the discussion of fig. 9 of ref. [3] for a more detailed description.)

Here and throughout this paper, we will often denote the measurement operator $j^{(3)\mu}$ by simply j^μ when there is small chance of confusion.

The charge deposition function $\hat{\Theta}(x)$ is only significant very close to the line $x^0 = x^3$ of travel of the high-energy jet. We shall not concern ourselves with the detailed profile of the width of this function. And so, following ref. [3], we will write

$$\langle \hat{\Theta}(x) \rangle_{A_{\text{cl}}} \simeq \delta_L(x^-) \langle \hat{\Sigma}_\Theta(t=\infty, \mathbf{x}) \rangle_{A_{\text{cl}}}, \quad (2.16a)$$

where

$$\hat{\Sigma}_\Theta(x) \equiv \int_{-\infty}^t dt' \hat{\Theta}(t', \mathbf{x}), \quad (2.16b)$$

and the L subscript on $\delta_L(x^-)$ indicates that the δ -function approximates a function whose width is of order L .

See ref. [3] for qualitative discussion of what the functions $\hat{\Theta}(x)$ and $\hat{\Sigma}_\Theta(x)$ look like. Here we will just summarize that the fact that net charge deposition is restricted to a region near the light cone, as shown by the cartoon picture of $\langle \hat{\Theta}(x) \rangle$ in Fig. 3a, means that the time-integrated charge deposition $\langle \hat{\Sigma}_\Theta(x) \rangle$ will be constant in time for times well inside the light-cone, as depicted in Fig. 3b. We can summarize this constancy as

$$\langle \hat{\Sigma}_\Theta(t=x^3+\epsilon, x^3) \rangle_{A_{\text{cl}}} \simeq \langle \hat{\Sigma}_\Theta(t=\infty, x^3) \rangle_{A_{\text{cl}}} \quad (2.17)$$

whenever $\epsilon \gg L$. The important thing to remember is that even though we will find it convenient to talk about and calculate $\hat{\Sigma}_\Theta(t=\infty, x^3)$, that quantity is determined by charge deposition that takes place at $t \simeq x^3$, not at $t = \infty$.

The great advantage of phrasing the problem in terms of the $t \rightarrow \infty$ limit of $\hat{\Sigma}_\Theta(x)$ is that the calculation in the gravity dual turns out to then only depend on the behavior of the corresponding 5-dimensional excitation at late times, when it has fallen very close to the

event horizon of the black hole. For the purpose of calculation, 5-dimensional propagators in Witten diagrams turn out to be much simpler and easier to deal with when the bulk points are very close to the horizon.

It's important to note that most of the time, a localized, small-amplitude source will not have any effect at all on the plasma. It is only on rare occasions, proportional to the square $|\mathcal{A}|^2$ of the source amplitude, that the source will create an excitation. When it does, the excitation will have the quantum numbers of the source. The jets will have energy and momentum $\simeq E$. Their R charge e_{jet} will be the R charge of the source operator,⁴ which is $e_{\text{jet}}=1$ for the specific choice (2.5b) and may take other values for the examples discussed in Appendix A. The average charge created in response to the source,

$$\mathcal{Q} \equiv \int d^3x \langle j^{(3)0}(x) \rangle_{A_{\text{cl}}} \Big|_{x^0 \gg L}, \quad (2.18)$$

is therefore e_{jet} times the probability \mathcal{P}_{jet} that a jet is created. In general, we will be interested in average charge densities and charge deposition *in the case that a jet has actually been created*. We can factor out the probability of creating the jet in the first place by defining expectations

$$\langle \dots \rangle_{\text{jet}} \equiv \frac{\langle \dots \rangle_{A_{\text{cl}}}}{\mathcal{P}_{\text{jet}}} = \frac{\langle \dots \rangle_{A_{\text{cl}}}}{\mathcal{Q}/e_{\text{jet}}}. \quad (2.19)$$

So, in the notation of this paper, the average charge deposition of our jets is given by

$$\langle \hat{\Theta}(x) \rangle_{\text{jet}} = \frac{\langle \hat{\Theta}(x) \rangle_{A_{\text{cl}}}}{\mathcal{Q}/e_{\text{jet}}}. \quad (2.20)$$

Finally, at a practical level, the calculation of the Green function in (2.11) took advantage of approximations based on the momentum scales relevant to the problem. Since we measure where the charge is deposited by its subsequent diffusion, and since diffusion is a hydrodynamic process that takes place on distance and time scales large compared to the mean-free path and so large compared to $1/T$, we do not need to resolve the structure of $\langle j^{(3)0}(x) \rangle$ on scales as small as $1/T$. In particular, we do not need to know the integrand of (2.12) except for when the components of Q (the 4-momentum conjugate to the measurement position x) are small compared to T . In contrast, the momenta Q_1 and Q_2 associated with the source factors in (2.12) are both large compared to T because we have chosen a high-energy/high-momentum source. That means that, after Fourier transforming the boundary points, the (red) propagators associated with the source points x_1 and x_2 in the Witten diagram of fig. 2a will have high 4-momentum, and so can be treated in a WKB-like approximation, whereas the (blue) propagator associated with the measurement point x will have low 4-momentum, which also allows for simplification. Similar simplifications will occur when calculating 4-point correlators such as fig. 2b.

⁴ Here and throughout, when we talk about the R charge e_{jet} of a jet, we mean the charge corresponding to the specific U(1) subgroup of SU(4) that we have chosen for our measurement operator, i.e. the charge corresponding to what we have labeled $j^{(3)0}$ in (2.10) and (2.18).

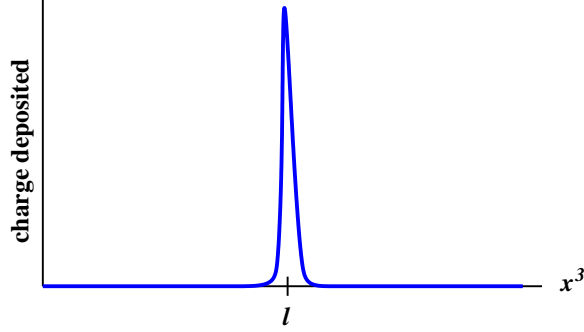


FIG. 4: A qualitative picture of charge deposition in a single event if charge deposition is very localized on an event-by-event basis. In this case, the location l of where the charge is deposited would have a probability distribution given by fig. 1.

D. The Measurement: This Paper

1. A first attempt

To motivate our calculation, imagine that we used a source that creates jets with large R charge ($e_{\text{jet}} \gg 1$). Then ask whether, in a single typical event, the spatial distribution of deposited charge looks like (i) fig. 1 or (ii) fig. 4. In the latter case, fig. 1 would give the probability distribution for the position l in fig. 4. Naively, a simple way to distinguish these two cases would be to measure the average correlation

$$\langle \hat{\Theta}(x) \hat{\Theta}(y) \rangle_{\text{jet}} = \frac{\langle \hat{\Theta}(x) \hat{\Theta}(y) \rangle_{A_{\text{cl}}}}{Q/e_{\text{jet}}} \quad (2.21)$$

for well separated x and y . The idea is that, for well separated x and y , case (i) would give

$$\langle \hat{\Theta}(x) \hat{\Theta}(y) \rangle_{\text{jet}} \simeq \langle \hat{\Theta}(x) \rangle_{\text{jet}} \langle \hat{\Theta}(y) \rangle_{\text{jet}}, \quad (2.22)$$

whereas case (ii) would instead give

$$\langle \hat{\Theta}(x) \hat{\Theta}(y) \rangle_{\text{jet}} \simeq 0 \quad (2.23)$$

if x and y were much further apart than the width the peak in fig. 4.

When discussing correlators, there are operator ordering considerations except in the classical limit. Note, for instance, that the right-hand side of (2.22) is (i) symmetric with respect to $x \leftrightarrow y$ and (ii) real, whereas the left-hand side is not precisely either. Factorization such as (2.22) would require the imaginary part of the correlator to be small. The real and imaginary parts of $\langle \hat{\Theta}(x) \hat{\Theta}(y) \rangle$ are given respectively by the symmetric combination $\frac{1}{2} \langle \{ \hat{\Theta}(x), \hat{\Theta}(y) \} \rangle$ and the commutator $-i \frac{1}{2} \langle [\hat{\Theta}(x), \hat{\Theta}(y)] \rangle$. In this paper, we will focus on the real part, for which the two cases distinguished above would be

$$\frac{1}{2} \langle \{ \hat{\Theta}(x), \hat{\Theta}(y) \} \rangle_{\text{jet}} \simeq \langle \hat{\Theta}(x) \rangle_{\text{jet}} \langle \hat{\Theta}(y) \rangle_{\text{jet}} \quad (2.24)$$

and

$$\frac{1}{2} \langle \{ \hat{\Theta}(x), \hat{\Theta}(y) \} \rangle_{\text{jet}} \simeq 0. \quad (2.25)$$

As we will see in a moment, the idea for our correlation measurement will require a little bit of refinement, but the basic goal of this paper is to demonstrate a refined version of (2.25) and so verify that the deposition of charge by a jet looks like fig. 4 on an event-by-event basis with a width $\Delta x^3 \lesssim 1/T$. We will refer to this as “localized” deposition of charge.

Eqs. (2.24) and (2.25) lay out two logical extremes for how a correlation might behave, but *a priori* the truth could instead lie somewhere in between. In particular, factorization (2.24) is not a very plausible option for non-local correlations unless $e_{\text{jet}} \gg 1$. But the simple question of whether the correlation is local or non-local can be sensibly asked for $e_{\text{jet}}=1$ as well as $e_{\text{jet}} \gg 1$. In the main text, for the sake of concreteness and compatibility with previous work, we will focus on the case $e_{\text{jet}}=1$ corresponding to the specific source (2.5b). For the sake of completeness, we will discuss the same question for $e_{\text{jet}} \gg 1$ in Appendix A. In both cases, we will find locality for the suitably-refined correlation.

In calculations, we will find it easier to study the correlator

$$\frac{1}{2} \langle \{ \hat{\Sigma}_{\Theta}(x^0=\infty, \mathbf{x}), \hat{\Sigma}_{\Theta}(y^0=\infty, \mathbf{y}) \} \rangle \quad (2.26)$$

of time-integrated charge-deposition (2.16b) rather than $\frac{1}{2} \langle \{ \hat{\Theta}(x), \hat{\Theta}(y) \} \rangle$ directly.

2. Refinement

When we later evaluate the correlation $\frac{1}{2} \langle \{ \hat{\Theta}(x), \hat{\Theta}(y) \} \rangle$ in the gravity dual, we will see that we want to throw out certain types of diagrammatic contributions which do not have the causal structure appropriate for the question of how charge deposition from a jet is correlated. In this section, we discuss what goes wrong if one includes all contributions to $\frac{1}{2} \langle \{ \hat{\Theta}(x), \hat{\Theta}(y) \} \rangle$, and we outline a more careful definition of charge deposition which avoids unwanted contributions and only includes the physics of interest.

From our definition (2.15) of charge deposition $\hat{\Theta}(x)$, the correlator we proposed above for study is

$$\frac{1}{2} \langle \{ \hat{\Theta}(x), \hat{\Theta}(y) \} \rangle_{\text{jet}} = (\partial_{x^0} - D \nabla_{\mathbf{x}}^2) (\partial_{y^0} - D \nabla_{\mathbf{y}}^2) \frac{1}{2} \langle \{ j^0(x), j^0(y) \} \rangle_{\text{jet}}. \quad (2.27)$$

This would be fine if the only source of charge in the system contributing to this correlator were the charge deposited by the jet. However, even if there were no jet at all, the equilibrium correlator $\langle \{ j^0(x), j^0(y) \} \rangle_{\text{eq}}$ would be non-vanishing and would measure the correlation of charge-density fluctuations in the plasma. Not only is the equilibrium correlation not the physics we want to measure for studying jet stopping but, unlike the case of charge deposition, its time dependence is not the simple retarded time-dependence of the diffusion equation implicitly assumed in the introduction (2.13) of the charge deposition distribution $\hat{\Theta}(x)$. To see this, consider that the equilibrium charge density correlation function $\langle \{ j^0(x), j^0(y) \} \rangle_{\text{eq}}$ can be related to the retarded charge density correlator via the fluctuation-dissipation theorem:⁵

$$\frac{1}{2} \langle \{ j^0, j^0 \} \rangle_{\text{eq}} = -\text{cth}(\frac{1}{2}\beta\omega) \text{Im} G_{\text{R}}^{00}(\omega, \mathbf{q}), \quad (2.28)$$

⁵ See, for example, the discussion by Kubo [13]. Eq. (2.28) above is a special case of our later (3.3).

where we work in 4-momentum space (ω, \mathbf{q}) . In the hydrodynamic limit of small frequency and momentum, $G_R^{00} \propto D\mathbf{q}^2/(-i\omega + D\mathbf{q}^2)$ has retarded diffusive behavior, and (2.28) gives

$$\frac{1}{2}\langle\{j^0, j^0\}\rangle_{\text{eq}} \simeq \frac{2T}{\omega} \text{Im} \left(\frac{\chi}{T} \frac{D\mathbf{q}^2}{(-i\omega + D\mathbf{q}^2)} \right) = \frac{2\chi D\mathbf{q}^2}{\omega^2 + (D\mathbf{q}^2)^2}, \quad (2.29)$$

where χ is the charge susceptibility.⁶ It's useful to also write this as

$$\frac{1}{2}\langle\{j^0, j^0\}\rangle_{\text{eq}} \simeq \frac{2\chi}{i\omega} \left[\frac{D\mathbf{q}^2}{-i\omega + D\mathbf{q}^2} - \frac{D\mathbf{q}^2}{i\omega + D\mathbf{q}^2} \right]. \quad (2.30)$$

There is not only a diffusive pole $-i\omega + D\mathbf{q}^2 = 0$ but also a conjugate pole $i\omega + D\mathbf{q}^2 = 0$ corresponding to its time reversal. Multiplying both sides by factors of $-i\omega + D\mathbf{q}^2$ to turn j^0 's into $\hat{\Theta}$'s would simplify the first term of (2.30) but not the second. The difficulty is that the correlation represented by $\langle\{j^0, j^0\}\rangle_{\text{eq}}$ is time symmetric, unlike the diffusion operator $\partial_t - D\nabla^2$ and unlike the physics of charge that is suddenly deposited in the medium by a thermalizing jet and only subsequently diffuses. The upshot is that the equilibrium contribution to $\langle\{j^0(x), j^0(y)\}\rangle_{\text{eq}}$ messes up our desired physical interpretation of the correlation (2.27).

There is a simple fix to the problem identified so far: Subtract out the equilibrium contribution to the charge correlation, and so study

$$(\partial_{x^0} - D\nabla_{\mathbf{x}}^2)(\partial_{y^0} - D\nabla_{\mathbf{y}}^2) \left[\langle\{j^0(x), j^0(y)\}\rangle_{\text{jet}} - \langle\{j^0(x), j^0(y)\}\rangle_{\text{eq}} \right] \quad (2.31)$$

instead of (2.27).

But there is still a problem. Consider the case where the jet passes through a region of plasma that contains some equilibrium fluctuation in the charge density. It's conceivable that interaction with that fluctuation, depending on its sign, could bias the probability that the jet stops earlier or later, as depicted in fig. 5. So we could get a contribution to (2.27) where the $j^0(x)$, for example, represents a pre-existing charge fluctuation in the plasma (i.e. not something caused by the jet) and the $j^0(y)$ represents diffusion from a jet depositing its charge at y . Let's call this a plasma-jet contribution to the correlation. Such a contribution would contaminate what we really want to know, which is the correlation between the jet depositing its charge at x and depositing its charge at y . Plasma-jet contributions to the correlation would also not give the retarded time dependence in x^0 assumed by the $(\partial_{x^0} - D\nabla_{\mathbf{x}}^2)$ factor in (2.27) for the same physical reason as in the discussion of the purely equilibrium correlator $\langle\{j^0(x), j^0(y)\}\rangle_{\text{eq}}$. This vague concern will be made concrete when we later discuss diagrammatic contributions to (2.27) in the (r,a) formalism. We will see that some diagrams correspond to the physics of the charge deposition correlation that we want, while other diagrams correspond to plasma-jet correlations that we are not interested in for the purposes of answering our question about how charge is deposited.

⁶ The overall normalization of the right-hand side of (2.29) is determined by integrating both sides $d\omega/2\pi$ over all ω and then taking $\mathbf{q} \rightarrow 0$. After this procedure, the left-hand side becomes the equal-time expectation $\langle(\text{total charge})^2\rangle/\text{volume}$, which defines the charge susceptibility χ . For a more specific formula for the hydrodynamic limit of $G_R^{00}(\omega, \mathbf{q})$ for $\mathcal{N}=4$ SYM in particular, see, for example, eq. (79) in the review article [1].

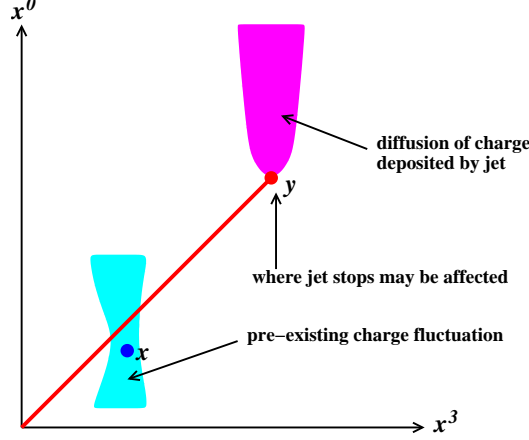


FIG. 5: A cartoon depicting a possible correlation between a charge fluctuation in the plasma at x and the deposition of the jet's charge at y .

Since neither the original correlator $\frac{1}{2}\langle\{\hat{\Theta}(x), \hat{\Theta}(y)\}\rangle$ nor the subtracted version (2.31) exactly capture the physics we want, how can we define something that does? The problem is that our definition of charge deposition as given by (2.15) for $\hat{\Theta}(x)$ is not really a good definition of charge deposition when we want to study correlators. We should define more carefully what it means for the jet to deposit charge somewhere. Here is one way to do that. Until the jet deposits its charge, we know from previous work that it stays close to the light-cone $x^0 = x^3$, within a distance $x^- \sim L$ (assuming $L \gtrsim 1/T$). We wish to define the net charge density deposited by the jet in the vicinity of some point \bar{x}^+ along the light-cone. Consider two 3-dimensional hyper-planar strips defined by

$$x^- = \pm\delta_{\text{plane}}, \quad |x^+ - \bar{x}^+| \leq \ell_{\text{plane}}, \quad (2.32)$$

corresponding to the dashed lines in fig. 6a. Choose δ_{plane} and ℓ_{plane} so that $L \ll \delta_{\text{plane}} \ll \ell_{\text{plane}} \ll \Delta x^+$, where Δx^+ is whatever scale at which one wants to resolve differences between stopping distances. Δx^+ should definitely be chosen small compared to the typical stopping distance $(EL)^{1/4}/T$. Consider the space-time region bounded by the two planes and approximately define the charge deposited at \bar{x}^+ as the difference between the charge leaving that region through the top plane and entering it through the bottom plane:

$$\begin{aligned} \bar{\Sigma}_{\Theta}(\infty, x^3 = \frac{1}{2}\bar{x}^+) &\equiv \frac{1}{\ell_{\text{plane}} V_{\perp}} \int dS_{\mu} j^{\mu} \\ &= \frac{1}{\ell_{\text{plane}}} \int_{\bar{x}^+ - \frac{1}{2}\ell_{\text{plane}}}^{\bar{x}^+ + \frac{1}{2}\ell_{\text{plane}}} \frac{dx^+}{2} \int \frac{d^2 \mathbf{x}^{\perp}}{V_{\perp}} \left[j^- \left(\frac{x^+ - \delta_{\text{plane}}}{2}, \mathbf{x}^{\perp}, \frac{x^+ + \delta_{\text{plane}}}{2} \right) \right. \\ &\quad \left. - j^- \left(\frac{x^+ + \delta_{\text{plane}}}{2}, \mathbf{x}^{\perp}, \frac{x^+ - \delta_{\text{plane}}}{2} \right) \right], \end{aligned} \quad (2.33)$$

where the dS integral in the first line is over both hyper-plane segments, with dS_{μ} pointing outward from the region between, and V_{\perp} is the area of the transverse dimensions \mathbf{x}_{\perp} .⁷

⁷ Remember that we have chosen to set up a transverse translationally invariant problem, so V_{\perp} is just an

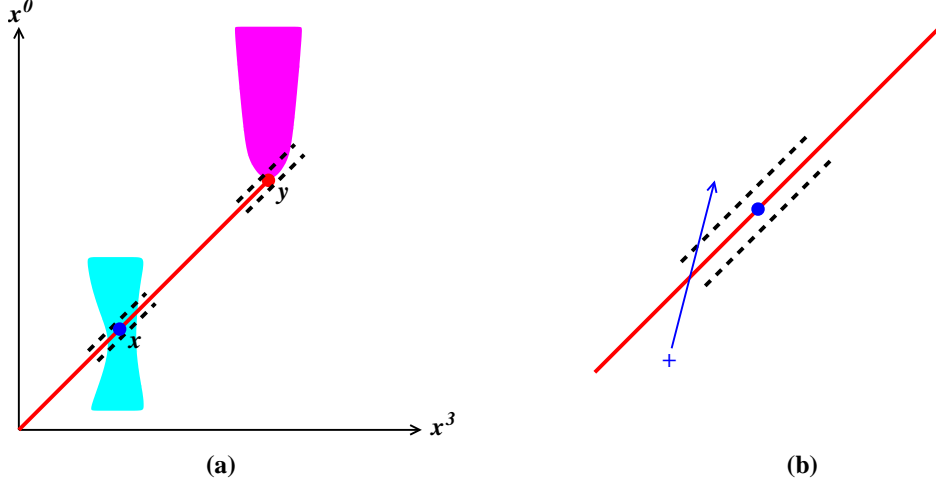


FIG. 6: (a) The hyper-plane segments (dashed lines) used to define $\bar{\Sigma}_\Theta$ corresponding to charge deposition near the light-cone points x and y . (b) An enlarged picture of one set of these planes showing how a charge fluctuation from the plasma might sneak between a pair of planes through one of the open ends and so be wrongly counted in the charge deposition measurement.

The jet sneaks into the region, without crossing either plane, through the lower-left opening between the planes in fig. 6a. If it does not thermalize there, then it sneaks out again, uncounted, through the upper-right opening. If some or all of its charge thermalizes in the region, that deposition of charge will be counted by (2.33). This definition solves the problem of jet-plasma correlations because a pre-existing charge fluctuation in the vicinity of x will give a canceling contribution to (2.33) between passing through the lower and upper planes, as depicted in fig. 6a. There will be errors in this procedure because of edge effects: some fluctuation in the equilibrium charge density might sneak in one side and be counted, as shown in fig. 6b. But such effects will scale away as one makes ℓ_{plane} larger and so can be disentangled.

We use the bar over Σ_Θ in (2.33) to distinguish our refined version of $\hat{\Sigma}_\Theta(\infty, x^3)$ from our original definition (2.16b). The bar can also crudely be thought of indicating that this definition averages $\hat{\Sigma}_\Theta(\infty, x^3)$ over a distance of order ℓ_{plane} , and so introduces some smearing. Such smearing is inconsequential as long as one keeps ℓ_{plane} small compared to the differences in stopping distances that one wishes to resolve. Finally, we remind the reader that the quantity $\Sigma_\Theta(\infty, x^3)$ arises from charge that is deposited near the light-cone $x^0 \simeq x^3$ and not at $x^0 = \infty$. See (2.17).

Consider now yet another possible source of $\langle \{j^0(x), j^0(y)\} \rangle$ correlation. When the jet stops, it deposits energy and momentum into the medium, which can then propagate away in the form of sound waves. These sound waves locally increase and decrease the temperature and pressure as they pass by. A small change δT in local temperature will give a small,

infinite (and uninteresting) normalization factor. Eq. (2.33) really defines the \mathbf{x}_\perp -averaged time-integrated charge deposition function. We could have equally well defined the symbol Σ_Θ throughout this paper to be the \mathbf{x}_\perp -integrated (rather than averaged) time-integrated charge density, in which case there would be no $1/V_\perp$ factors in (2.33).

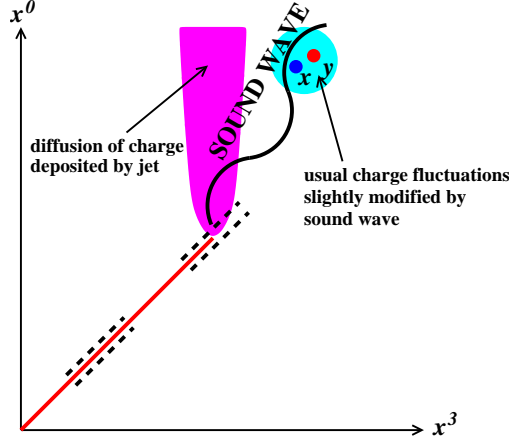


FIG. 7: A jet travels along the light cone and then deposits its charge, which diffuses, as well as sound energy, which propagates. The local oscillation of temperature associated with the sound wave can then modify the local correlations between $j^0(x)$ and $j^0(y)$ at, for example, the points shown. Such a change in the correlation would contribute to (2.31) but is invisible to the refined measurement (2.33), which is defined specifically for x and y on the light cone and only involves j^0 at points close to the light cone, such as at the dashed lines.

local change to the contribution to $\langle\{j^0(x), j^0(y)\}\rangle$ in that region from finite-temperature fluctuations of the plasma there, leading, for example, to a contribution

$$(\partial_{x^0} - D\nabla_{\mathbf{x}}^2)(\partial_{y^0} - D\nabla_{\mathbf{y}}^2) \left[\langle\{j^0(x), j^0(y)\}\rangle_{\text{eq}, T+\delta T} - \langle\{j^0(x), j^0(y)\}\rangle_{\text{eq}, T} \right] \quad (2.34)$$

to the subtracted correlator (2.31). We will later see a Witten diagram in the gravity dual calculation which naturally produce this sort of effect. Fortunately, our refined measurement (2.33) would eliminate this contribution since it only looks at charge density near the light cone and so is not affected by effects on the charge density far away, such as shown in fig. 7.

The definition (2.33) is an example of how to define charge deposition, but it would be awkward and difficult to compute $\frac{1}{2}\langle\{\bar{\Sigma}_{\Theta}(\infty, x^3), \bar{\Sigma}_{\Theta}(\infty, y^3)\}\rangle$ using this detailed formula in practice. However, we will see that its effect is to simply eliminate certain types of (gravity dual) diagrammatic contributions to the charge-charge correlation and to reproduce our naive $\frac{1}{2}\langle\{\hat{\Sigma}_{\Theta}(\infty, x^3), \hat{\Sigma}_{\Theta}(\infty, y^3)\}\rangle$ for the diagrammatic contributions which survive. The upshot is that in practice we will just compute

$$\left[\frac{1}{2}\langle\{\hat{\Sigma}_{\Theta}(\infty, \mathbf{x}), \hat{\Sigma}_{\Theta}(\infty, \mathbf{y})\}\rangle_{\text{jet}} \right]_{\text{relevant diagrams}} \quad (2.35)$$

We will see which are the relevant diagrammatic contributions in sec. III D.

III. 4-POINT FUNCTIONS AND DIAGRAMMATIC SETUP

In this section, we see precisely which type of 4-point equilibrium correlator we need to calculate and how it corresponds to an appropriately causal real-time Witten diagram in the gravity dual. But first, it will be convenient to review the (r,a) notation for organizing the classification of real-time correlators, based on Schwinger-Keldysh formalism.

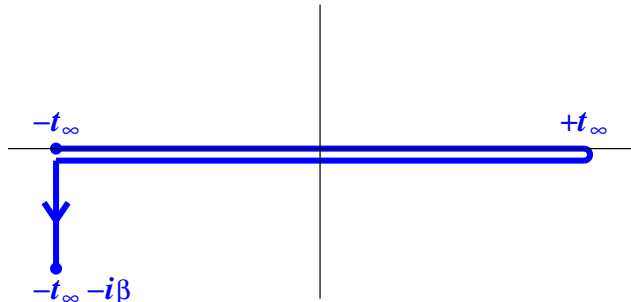


FIG. 8: The Schwinger-Keldysh contour in the complex time plane.

A. Field theory review of (r,a) notation

(r,a) notation is nicely summarized in ref. [14], and examples of its application to calculations with gauge-gravity duality may be found in refs. [10, 15, 16]. One begins with Schwinger-Keldysh formalism for a system in thermal equilibrium, where the finite-temperature imaginary-time integration contour from 0 to $-i\beta$ is deformed into real time as shown in fig. 8.⁸ Operators may be placed on either the upper or lower horizontal sections of the path, with operators labeled type “1” or “2” correspondingly, and the n -point functions are then path ordered. For example, consider the n -point correlator of a single field $O(x)$. Then

$$\begin{aligned} i^4 G_{12212}(x_1, x_2, x_3, x_4, x_5) &\equiv \langle \mathcal{T}_P [O_1(x_1) O_2(x_2) O_2(x_3) O_1(x_4) O_2(x_5)] \rangle \\ &\equiv \langle \bar{\mathcal{T}} [O(x_2) O(x_3) O(x_5)] \mathcal{T} [O(x_1) O(x_4)] \rangle, \end{aligned} \quad (3.1)$$

where \mathcal{T}_P is Schwinger-Keldysh path ordering and \mathcal{T} and $\bar{\mathcal{T}}$ represent ordinary time ordering and reverse time ordering respectively. For 2-point functions, G_{11} is the Feynman propagator G_F ; G_{22} is related to G_F^* ; and G_{12} and G_{21} are the Wightman correlators $G_<$ and $G_>$.

The (r,a) notation consists of switching the basis of the labels 1 and 2 to⁹

$$O_a \equiv O_1 - O_2, \quad O_r \equiv \frac{1}{2}(O_1 + O_2). \quad (3.2a)$$

We will define the corresponding n -point Green functions by

$$i^{n-1} G_{\alpha_1 \dots \alpha_n}(x_1, \dots, x_n) = 2^{n_r-1} \langle \mathcal{T}_P [O_{\alpha_1}(x_1) \dots O_{\alpha_n}(x_n)] \rangle, \quad (3.2b)$$

where each α_i is either “r” or “a” and n_r is the number of “r” indices. Different authors use different factor of 2 conventions, and ours are those of Wang and Heinz [14]. For 2-point functions, $G_{\text{ar}}(0, x)$ is the retarded Green function $G_R(x)$; $G_{\text{ra}}(0, x)$ is the advanced

⁸ People sometimes find it useful to deform the contour so that there is a vertical segment that drops from $+t_\infty$ to $+t_\infty - i\sigma$ on the right-hand side of fig. 8, and then the vertical segment on the left-hand side drops from $-t_\infty - i\sigma$ to $-t_\infty - i\beta$. For instance, ref. [18] uses $\sigma = \beta/2$. But here we will stick with the traditional $\sigma = 0$.

⁹ In the literature on the Schwinger-Keldysh formalism, O_a and O_r are sometimes referred to, up to factor of 2 normalization conventions, as the “quantum” and “classical” fields O_q and O_{cl} respectively. See, for example, ref. [15, 19].

Green function $G_A(x)$; $iG_{\text{rr}}(0, x)$ is the symmetric correlator $\langle\{O(0), O(x)\}\rangle = iG_{>} + iG_{<}$; and $G_{\text{aa}} = 0$. An equilibrium relation that we will find useful later on is the fluctuation-dissipation theorem,

$$iG_{\text{rr}}(\omega, \mathbf{q}) = -2 \text{cth}(\frac{1}{2}\beta\omega) \text{Im} G_{\text{R}}(\omega, \mathbf{q}) = \text{cth}(\frac{1}{2}\beta\omega) [iG_{\text{R}}(\omega, \mathbf{q}) - iG_{\text{A}}(\omega, \mathbf{q})] \quad (3.3)$$

for bosonic correlators,¹⁰ which we have previously referenced in (2.28).

Here is a useful property of correlators in (r,a) notation:

Rule 1. An n -point function vanishes if the largest time $\max(t_1, \dots, t_n)$ is associated with an operator O_{a} that has an ‘‘a’’ label.

This follows because, if x^0 is the largest time in the correlation, then there is no difference between the operator ordering of $\phi_1(x)$ and $\phi_2(x)$, and so $\phi_{\text{a}}(x)$ defined by (3.2a) vanishes. Rule 1 has the following corollary:

Rule 2. The n -point function $G_{\text{aa}\dots\text{a}}$ with all ‘‘a’’ labels is zero.¹¹

It is also useful to take note of a property of perturbation theory in (r,a) formalism, even though the 4-dimensional field theory we are interested in (strongly-coupled $\mathcal{N}=4$ super Yang-Mills) is not weakly coupled. In the Schwinger-Keldysh formalism, using the time contour of fig. 8, the path integral schematically takes the form

$$\int [\mathcal{D}\phi_1(x)][\mathcal{D}\phi_2(x)] e^{i\int_x (\mathcal{L}[\phi_1] - \mathcal{L}[\phi_2])} e^{-S_{\text{E}}[\phi_3]}, \quad (3.4)$$

where ϕ_1 and ϕ_2 live on the upper and lower horizontal contour and ϕ_3 lives on the vertical stub of the contour at $\text{Re } t = -t_{\infty}$. In Hamiltonian language, the ϕ_1 and ϕ_2 parts respectively generate the evolution operators $e^{-i\int H dt}$ and $e^{+i\int H dt}$ that appear in the time evolution $e^{+i\int H dt} O e^{-i\int H dt}$ of operators that we wish to measure, while the ϕ_3 part generates the equilibrium density matrix $e^{-\beta H}$. Order by order in perturbation theory, there are generically corrections both to the evolution operators $e^{\pm i\int H dt}$ and to the initial density matrix $e^{-\beta H}$. For our application, only corrections to the evolution will turn out to be important, and so focus on the corresponding interaction terms

$$\int_x (V[\phi_1] - V[\phi_2]) = \int_x (V[\phi_{\text{r}} + \frac{1}{2}\phi_{\text{a}}] - V[\phi_{\text{r}} - \frac{1}{2}\phi_{\text{a}}]). \quad (3.5)$$

The integrand is odd in ϕ_{a} . As a result we have the following rule in (r,a) notation:

Rule 3. Any interaction vertex (associated with time evolution) must have an odd number of ‘‘a’’ fields.

¹⁰ In addition to Kubo [13], see, for example, eq. (32) of Wang and Heinz [14]. Also $iG_{>}(\omega, \mathbf{q}) = -2[n(\omega) + 1] \text{Im} G_{\text{R}}(\omega, \mathbf{q})$ and $iG_{<}(\omega, \mathbf{q}) = -2n(\omega) \text{Im} G_{\text{R}}(\omega, \mathbf{q})$, where $n(\omega) = 1/(e^{\beta\omega} - 1) = \frac{1}{2}[\text{cth}(\frac{1}{2}\beta\omega) - 1]$ is the Bose distribution function. For a textbook reference, see, for example, eq. (7.6.41) of ref. [20], where their $2\chi''$ is the commutator $\langle[O(x), O(x')]\rangle = iG_{\text{R}} - iG_{\text{A}}$ and their S is the Wightman function $iG_{>} = \langle O(x) O(x') \rangle$. By taking $\omega \rightarrow -\omega$ one gets the corresponding relation for $G_{<}$, and then adding $G_{>}$ and $G_{<}$ gives G_{rr} . As far as the case $\omega=0$ is concerned, we have implicitly assumed $\langle O \rangle = 0$, and so O should be replaced by $O - \langle O \rangle$ if not.

¹¹ This rule is equivalent to the largest-time diagrammatic identity of Veltman [21].

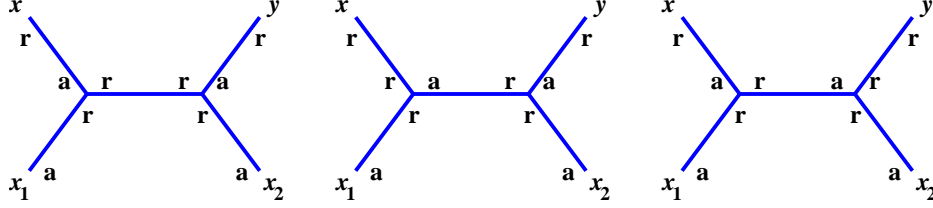


FIG. 9: The non-vanishing (r,a) assignments for the propagators in one of the diagrams that contribute to $G_{aarr}(x_1, x_2, x, y)$.

As a simple example, consider the contribution of the diagram of fig. 9 to the 4-point correlator $G_{aarr}(x_1, x_2, x, y)$. Applying Rules 1–3, the figure shows all the non-vanishing (r,a) assignments for this diagram’s contribution to G_{aarr} .

Of course, we will not be doing perturbation theory in 4-dimensional field theory for strongly-coupled $\mathcal{N}=4$ super Yang-Mills theory. However, as others before us [10, 16], we will extend the use of the (r,a) notation to organize calculations in the 5-dimensional gravitational dual theory. In the gravitational theory, we are doing perturbation theory. Because the 5-dimensional AdS₅-Schwarzschild background is periodic in imaginary time with period $2\pi T$, the methods of thermal field theory can be taken over to this 5-dimensional field theory problem [17].

Finally, returning for a moment to ordinary perturbative thermal quantum field theory, we should mention that there is a long, involved story about whether and how, in the limit $t_\infty \rightarrow \infty$, one may ignore vertices which correspond to interaction terms such as $(\phi_3)^3$ that live on the vertical stub of the contour in fig. 8. (See Gelis [22].) However, this is a subtlety which may be blissfully ignored in many applications of interest. For example, consider a diagram like fig. 10, where the “3” vertex represents a $(\phi_3)^3$ interaction along the vertical stub of the contour in fig. 8. This diagram is zero because, by the same logic that led to Rule 1, the propagator $G_{3a} = 0$. At leading order, there are no non-vanishing diagrams for G_{aarr} that involve corrections to the initial density matrix, and so all the vertices in fig. 9 just involve r’s and a’s. In the gravity dual, an analogous concern would arise if evaluating a correlator whose causality structure allowed bulk vertices to be inside the past or future horizon in fig. 2 and potentially touch the singularity, but this will not happen in our application. (When it does happen, ref. [23] shows how to evaluate correlators in a way that satisfies thermal equilibrium relations and does not require consideration of points inside the horizon. Alternatively, one may use equilibrium relations [14] to relate the correlator to another that avoids the problem. Or, as a matter of principle, one might use the complexified AdS₅-Schwarzschild of Skenderis and van Rees [24, 25].)

B. The desired 4-point correlator

In our earlier work [3], we needed an equilibrium 3-point retarded correlator $G_{aar}(x_1, x_2; x)$ to calculate the response $\langle j^0(x) \rangle_{A_{cl}}$ of charge density to the creation of a jet, where each of the “a” subscripts in G_{aar} is associated with the source operator. In this section, we will see that we need the equilibrium 4-point correlator $G_{aarr}(x_1, x_2; x, y)$ to calculate the correlator $\frac{1}{2} \langle \{j^0(x), j^0(y)\} \rangle_{A_{cl}}$. The appearance of “r” subscripts for both x and y in G_{aarr} can be thought of as a generalization of the equilibrium relation $iG_{rr} = \langle \{O(x), O(y)\} \rangle_{eq}$ to

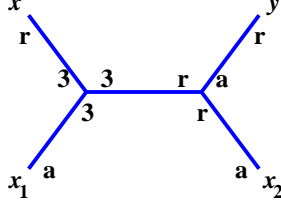


FIG. 10: An example of a diagram involving the fields ϕ_3 on the vertical stub of the Schwinger-Keldysh time path of fig. 8. Here the vertex marked with 3's represent a $(\phi_3)^3$ vertex on that stub. This assignment (and all other assignments of this diagram that involve ϕ_3 vertices) vanishes because $G_{3a} = 0$.

the case of jets created by a source A_{cl} .

Write the Hamiltonian of our system as $H(t) = H_0 + \delta H(t)$, where $\delta H(t)$ contains the small-amplitude source terms that we introduce to create the jet and H_0 is everything else in the full, interacting Hamiltonian of the theory. Take $\delta H(t)$ to be localized in time, as previously discussed, and assume the system starts in equilibrium at $t \rightarrow -\infty$. As reviewed in our earlier work [3], the response of an observable \mathcal{O} is given by the following expansion in δH :

$$\Delta\langle\mathcal{O}(t)\rangle \equiv \langle\mathcal{O}(t)\rangle_H - \langle\mathcal{O}\rangle_{H_0} = \int dt_1 G_{\text{ar}}(t_1; t) + \frac{1}{2!} \int dt_1 dt_2 G_{\text{aar}}(t_1, t_2; t) + \dots, \quad (3.6)$$

where the various $G_{\text{a}\dots\text{ar}}$ are the equilibrium n -point retarded correlation functions, given in this case by

$$iG_{\text{ar}}(t_1; t) = \theta(t - t_1) \langle[\mathcal{O}(t), \delta H(t_1)]\rangle_{H_0}, \quad (3.7)$$

$$i^2G_{\text{aar}}(t_1, t_2; t) = \theta(t - t_2) \theta(t_2 - t_1) \langle[[\mathcal{O}(t), \delta H(t_2)], \delta H(t_1)]\rangle_{H_0} \\ + \theta(t - t_1) \theta(t_1 - t_2) \langle[[\mathcal{O}(t), \delta H(t_1)], \delta H(t_2)]\rangle_{H_0}, \quad (3.8)$$

etc. Taking \mathcal{O} to be $j^{(3)\mu}(x)$, and δH from (2.5) to be $\int d^3x \mathbf{j} \cdot \mathbf{A}_{\text{cl}}$, reproduces the formula (2.11) that we reviewed earlier for $\langle j^{(3)\mu}(x) \rangle_{A_{\text{cl}}}$.

Nothing changes in the derivation of the above formulas if one replaces $\mathcal{O}(t)$ by a product of operators $\mathcal{O}(t)\mathcal{O}(t')$ in the particular case that t and t' are both after the time at which the source has turned off (so that the source does not affect the time evolution operator between t and t'). Such late-time observables are precisely what we're interested in for studying jet stopping. We will focus in particular on the symmetric product $\frac{1}{2}\{\mathcal{O}(t), \mathcal{O}(t')\}$ of measurement operators. In the case of interest to jet quenching—a high-momentum source δH and low-momentum observables \mathcal{O} —the leading contribution at post-source times to the δH expansion will then be

$$\frac{1}{2}\Delta\langle\{\mathcal{O}(t), \mathcal{O}(t')\}\rangle \simeq \frac{1}{2!} \int dt_1 dt_2 G(t_1, t_2; t, t') \quad (3.9)$$

with

$$i^2G(t_1, t_2; t, t') = \theta(t_2 - t_1) \langle[[\frac{1}{2}\{\mathcal{O}(t), \mathcal{O}(t')\}, \delta H(t_2)], \delta H(t_1)]\rangle_{H_0} \\ + (t_1 \leftrightarrow t_2). \quad (3.10)$$

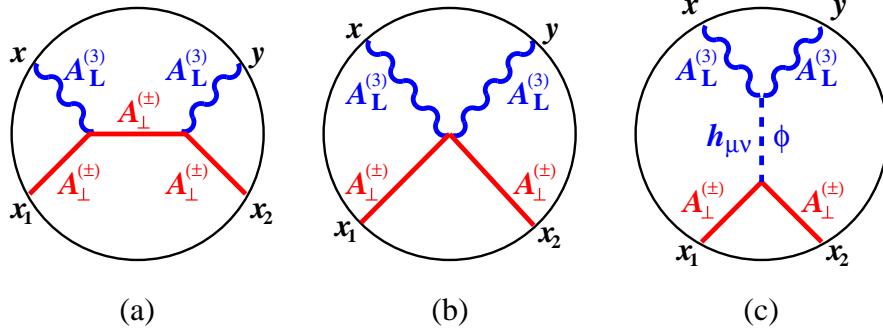


FIG. 11: Witten diagrams contributing to the 4-point current correlator in our problem, with the sources at the bottom and the measurement points x and y at the top. For (a), one should also add the diagram where x and y are interchanged. The types of lines are described in the text.

We have dropped factors such as $\theta(t-t_i)$ and $\theta(t'-t_i)$ because the formula (3.9) only applies in the case of post-source times, where t and t' are each greater than both t_1 and t_2 . In this case, it's easy to check that the (r,a) ordering rules described in section III A imply that G above is the same thing as $iG_{\text{aarr}}/2$. The factor of $i/2$ arises from our normalization convention (3.2) for (r,a) correlators.

Taking the same choices for \mathcal{O} and δH as before, we get the following 4-point generalization of the 3-point relation (2.11):

$$\frac{1}{2}\Delta\langle\{j^{(3)\mu}(x), j^{(3)\nu}(y)\}\rangle_{A_{\text{cl}}} = \frac{i}{4} \int d^4x_1 d^4x_2 G_{\text{aarr}}^{(ab33)\alpha\beta\mu\nu}(x_1, x_2; x, y) A_{\alpha, \text{cl}}^a(x_1) A_{\beta, \text{cl}}^b(x_2) \quad (3.11)$$

(for times x^0, y^0 after the source is turned off).

C. Witten diagrams in the gravity dual

Recall that we take our high-momentum source (2.5) to be translation invariant in the transverse directions (x^1, x^2) and transversely polarized. Restrict attention to measurements of correlators of the charge density j^0 , i.e. $\mu=\nu=0$ in (3.11). The Witten diagrams which contribute to the desired 4-point correlator in (3.11) are shown in fig. 11. (Here, for the sake of pictorial simplicity, we have not bothered to draw Penrose-diagram versions as in fig. 2.) We are also not yet implementing the ‘‘aarr’’ prescription on G_{aarr} , which we will discuss shortly. In these diagrams, straight solid lines represent propagators associated with the transverse polarizations A_{\perp} of the 5-dimensional gauge field. These have high 4-momentum and have index \pm in the $SU(2)$ subgroup of the $SU(4)$ R symmetry, corresponding to (2.5b). Wavy lines represent the $I=0$ and 3 components of the gauge field A_I (in $A_5=0$ gauge), which mix and which we've abbreviated as A_L in the figure. These wavy lines have low 4-momentum (since they are associated with our late-time measurement of diffusion) and index 3 in the $SU(2)$ R-symmetry subgroup. The dashed line can represent either a graviton or a massive scalar ϕ discussed by Romans [26].

As seen from fig. 11c, diagrams for the 4-point function can contain other supergravity (SUGRA) fields besides the ones dual to the boundary operators. The full set of fields in the SUGRA theory is rather complicated, but the problem of enumerating the diagrams can be

$$\begin{aligned}
G_{\mathbf{R}}(q) &= \text{a} \xrightarrow{q} \text{r} = \xrightarrow{q} \\
G_{\mathbf{A}}(q) &= \text{r} \xrightarrow{q} \text{a} = \xleftarrow{q} \\
G_{\mathbf{rr}}(q) &= \text{r} \xrightarrow{q} \text{r} = \xrightarrow{q} \parallel
\end{aligned}$$

FIG. 12: Our diagrammatic notation for propagators in the (r,a) formalism. The same convention is used for both bulk-to-bulk propagators $G^{(5)}$ and bulk-to-boundary propagators \mathcal{G} .

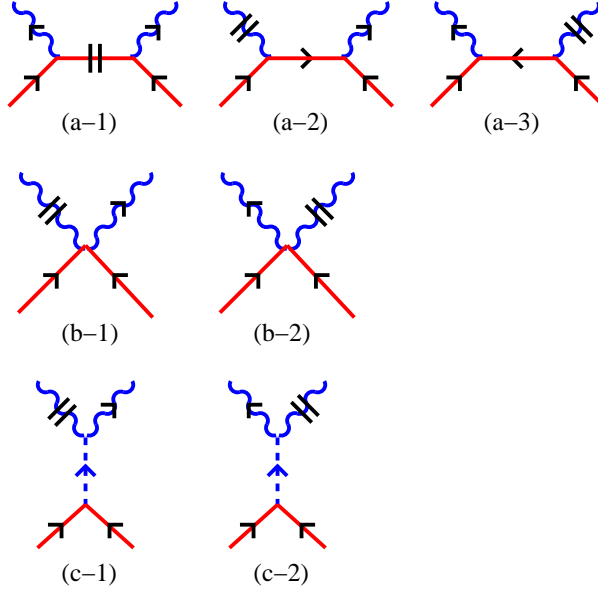


FIG. 13: Non-vanishing (r,a) assignments for Witten diagrams contributing to G_{aarr} in our problem. The first row is simply a rewriting of fig. 9 using the notation of fig. 12.

simplified due to the fact that our sources all lie in an $SU(2)$ subgroup of the full $SU(4)$ R symmetry. Lü, Pope, and Tran [27] showed that the 5-dimensional $SU(4)$ gauge theory in the gravity dual can be consistently truncated to a theory of just a $SU(2) \times U(1)$ subgroup, and the Lagrangian for $\mathcal{N}=4$ SUGRA in five dimensions with a gauged $SU(2) \times U(1)$ symmetry group is conveniently given by Romans [26]. However, none of the details matter because we will see later that only the diagram of fig. 11a will contribute to the physics we are interested in.

Now focus on G_{aarr} in particular. In order to depict (r,a) assignments graphically, we will use the notation defined in fig. 12. Using the rules of section III A, the (r,a) assignments for the diagrams of fig. 11 which contribute to G_{aarr} are shown in fig. 13. For comparison, the diagram corresponding to the 3-point function G_{aar} is shown in fig. 14.

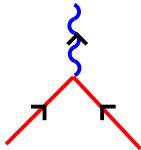


FIG. 14: Non-vanishing (r,a) assignment for the 3-point function G_{aar} .

D. The dominance of diagram (a-1)

We will now see that only diagram (a-1) potentially contributes to the physics of interest to us. The other diagrams, which all involve a \mathcal{G}_{tr} on one of the two measurement legs (the wavy lines), only contribute to plasma-jet and other correlations of the sort discussed and discarded in section IID 2. In all of the diagrams, we will make a low-momentum approximation for the 4-momenta Q and Q' conjugate to the measurement points x and y , as discussed at the end of section IIC. That is, we will blur our eyes and only concern ourselves with resolving measurements on distance and time scales larger than $1/T$.

We start by discussing some of the properties of diagram (a-1). The small 4-momentum limit of the gauge bulk-to-boundary propagator $\mathcal{G}_{I\mu}^{\text{R}}$ is given in refs. [1, 3].¹² The details do not matter yet except that the general form is

$$\mathcal{G}_{I\mu}^{\text{R}}(u; \omega, \mathbf{q}) = \frac{f_{I\mu}(u; \omega, \mathbf{q})}{i\omega - D\mathbf{q}^2}, \quad (3.12)$$

where each $f_{I\mu}(u; \omega, \mathbf{q})$ is polynomial in ω and \mathbf{q} (and so is local in 4-position space). Above, the pole $(i\omega - D\mathbf{q}^2)^{-1}$ describes diffusion according to the diffusion equation. If we now construct $\hat{\Theta}$ from j^0 for the measurement point, by multiplying (3.12) by $i\omega - D\mathbf{q}^2$ as in the definition (2.15) of $\hat{\Theta}$, we get

$$(\partial_t - D\nabla^2)\mathcal{G}_{I\mu}^{\text{R}} = \text{completely local in } x. \quad (3.13)$$

That is, in 4-position space, $(\partial_t - D\nabla^2)\mathcal{G}_{I\mu}^{\text{R}}$ connecting a bulk point (x', u) to a boundary point x only has support at $x=x'$ (up to the $1/T$ smearing of resolution intrinsic to our small-momentum approximation for the measurements). So, once we apply the diffusion operators $\partial_t - D\nabla^2$ to both measurement points as in (2.27), diagram (a-1) becomes a truncated diagram depicted by fig. 15a, with some derivatives and possibly u -dependent factors that correspond to $f_{I\mu}(u; \omega, \mathbf{q})$ above acting on the wavy stubs. If we drew a corresponding diagram for our earlier calculation [3] of $\langle \hat{\Theta}(x) \rangle_{A_{\text{cl}}}$, it would be fig. 15b. In that work, we found that the charge deposition only had support for x very close to the light cone, where close means within $\max(L, T^{-1})$. We will see the same thing happen in this paper in the calculation corresponding to fig. 15a. The underlying reason is that the 5-dimensional wave created by the source, given by a bulk-to-boundary propagator from a source point x_i (represented by a straight line from the boundary in figs. 13–15) convolved with the source wave packet $\Omega_L(x_i)e^{i\vec{k}\cdot x_i}$ on the boundary, stays close to the $x^0=x^3$ 4-space light cone for all times relevant to charge deposition ($x^0 \lesssim E^{1/3}$). We will leave the details of calculating the

¹² See in particular eq. (4.7) of ref. [3].

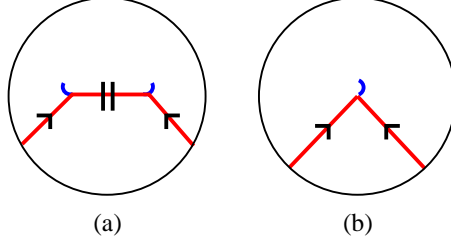


FIG. 15: Versions of fig. 13(a-1) and fig. 14 with the measurement bulk-to-boundary propagators truncated by applications of the diffusion operator $\partial_t - D\nabla^2$. We have included a depiction of the boundary in these figures to emphasize that the truncated vertices lie in the bulk.

contribution from diagram (a-1) until later, but this qualitative point about the truncated diagram will be enough to understand what happens with the other diagrams of fig. 13.

In diagram (a-1) of fig. 13, the charge-charge correlator $\frac{1}{2}\langle\{j^0(x), j^0(y)\}\rangle_{A_{cl}}$ was given by deposition near the light cone, represented by fig. 15a, propagated forward in time to the measurement points x and y by diffusive propagators, contained in the directed wavy lines in fig. 13(a-1). We depict this situation pictorially in fig. 16(a-1). What happens if instead one of those bulk-to-boundary propagators for x or y is a low-momentum \mathcal{G}_{rr} instead of a \mathcal{G}_R , as in diagram (a-2)? Applying (3.3) to the gravity calculation,

$$\begin{aligned} \mathcal{G}_{rr}(u; \omega, \mathbf{q}) &= \text{cth}(\frac{1}{2}\beta\omega) [\mathcal{G}_R(u; \omega, \mathbf{q}) - \mathcal{G}_A(u; \omega, \mathbf{q})] \\ &= \text{cth}(\frac{1}{2}\beta\omega) [\mathcal{G}_R(u; \omega, \mathbf{q}) - \mathcal{G}_R(u; -\omega, -\mathbf{q})]. \end{aligned} \quad (3.14)$$

As a result, $\mathcal{G}_{rr}(u; q)$ above is even under inversion $q \rightarrow -q$ of the 4-momentum. Fourier transforming in 4-space, that means that $\mathcal{G}_{rr}(x', u; x)$ is even in the difference $x - x'$ of the boundary and bulk 4-positions. We depict this situation pictorially in fig. 16(a-2), where the point associated with \mathcal{G}_{rr} has a backward-time diffusive region, corresponding to the second term in (3.14), that is PT -symmetric with the forward-time diffusive region. As a result, if we calculate the refined time-integrated charge-deposition operator $\bar{\Sigma}_\Theta$ of (2.33) at a point on the light cone, the contributions from subtracting the integrals of j^0 over the two dashed hyper-plane segments in the figure will cancel. And so diagram (a-2) will not contribute to our refined measure $\frac{1}{2}\langle\{\bar{\Sigma}_\Theta(\infty, x^3), \bar{\Sigma}_\Theta(\infty, y^3)\}\rangle$ of charge deposition correlations. The same conclusion holds for diagram (a-3) and, by similar logic, for (b-1) and (b-2).

In what follows, we will abbreviate $\bar{\Sigma}_\Theta(\infty, x^3)$ as $\bar{\Sigma}(x^3)$.

Now we come to the (symmetrically related) diagrams (c-1) and (c-2) of fig. 13. Focus on (c-1) for the sake of specificity and let (x', u) be the location of the top-most bulk vertex, as indicated in fig. 17. Because of the flow of causality (indicated by the arrows) from the source points x_1 and x_2 , the bulk point (x', u) must lie in the 5-dimensional causal future of x_1 and x_2 , and the measurement point y must lie in the future of that. This requires x' to be in the 4-dimensional causal future of the source and y to be in the causal future of x' . Now consider two cases: x' is (i) far from or (ii) near the $x^0 \simeq x^3$ lightcone, as in figs. 18a and b respectively. In the first case, it is causally impossible for the measurement point y to be near the light cone, and so there can be no contribution to the refined correlator $\frac{1}{2}\langle\{\bar{\Sigma}(x^3), \bar{\Sigma}(y^3)\}\rangle$, which is defined to only involve measurements near the light cone. In the second case, there can be a contribution but only if the measurement points x and y are very close to x' and so to each other. That's because y is connected to (x', u) by

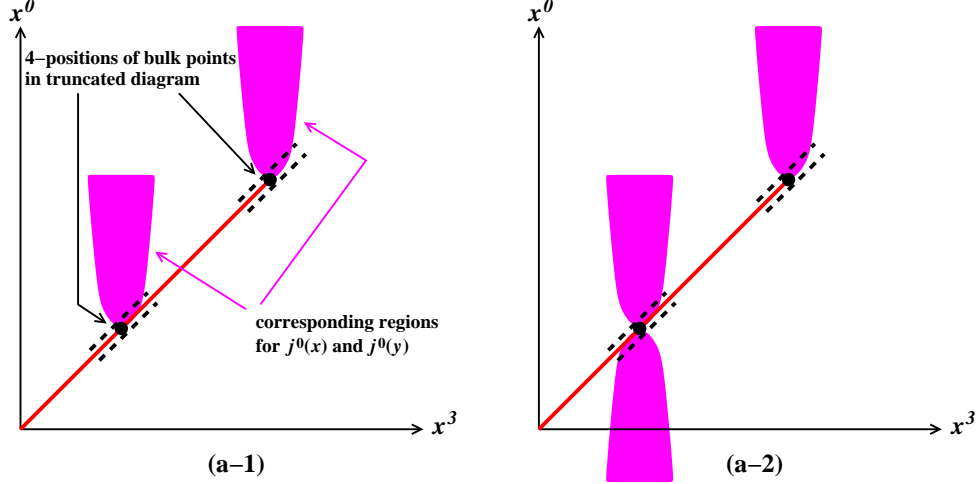


FIG. 16: Regions of x and y that contribute to the current correlator $\frac{1}{2}\langle\{j^0(x), j^0(y)\}\rangle$ when the bulk points, which lie near the light cone, have 4-positions indicated by the black dots. The two diagrams correspond to the cases of diagrams (a-1) and (a-2) of fig. 13.

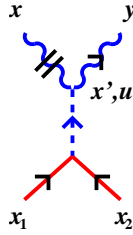


FIG. 17: Labeling of points for discussing diagram (c-1) of fig. 13.

a low-momentum \mathcal{G}_R and so must lie in the forward-time diffusive region relative to x' , as depicted by the magenta region in fig. 18b, while x is connected by a low-momentum \mathcal{G}_{tr} and so may lie in either the forward-time or backward-time regions, as depicted by the magenta and blue regions of fig. 18b. If both are to be measured close to light cone to determine $\frac{1}{2}\langle\{\bar{\Sigma}(x^3), \bar{\Sigma}(y^3)\}\rangle$, then all the points are close to each other, and so diagrams (c-1) and (c-2) only contribute to very localized correlations. Our goal, however, is to understand whether $\frac{1}{2}\langle\{\bar{\Sigma}(x^3), \bar{\Sigma}(y^3)\}\rangle$ has support at relatively large separations. To answer that question, we may therefore ignore (c-1) and (c-2).

The low-momentum graviton propagator has a sound pole.¹³ Though not necessary for the above argument, we note in passing that for a graviton internal propagator in (c-1), the picture in fig. 18a therefore plausibly has some relation to the type of physics discussed earlier in fig. 7.

The upshot of this section is that we may compute the refined correlator

¹³ See, for example, ref. [28], which derives sound poles in the bulk-to-boundary graviton propagator and then in 2-point boundary correlators. We will discuss later the relation of bulk-to-boundary and bulk-to-bulk propagators at finite temperature.

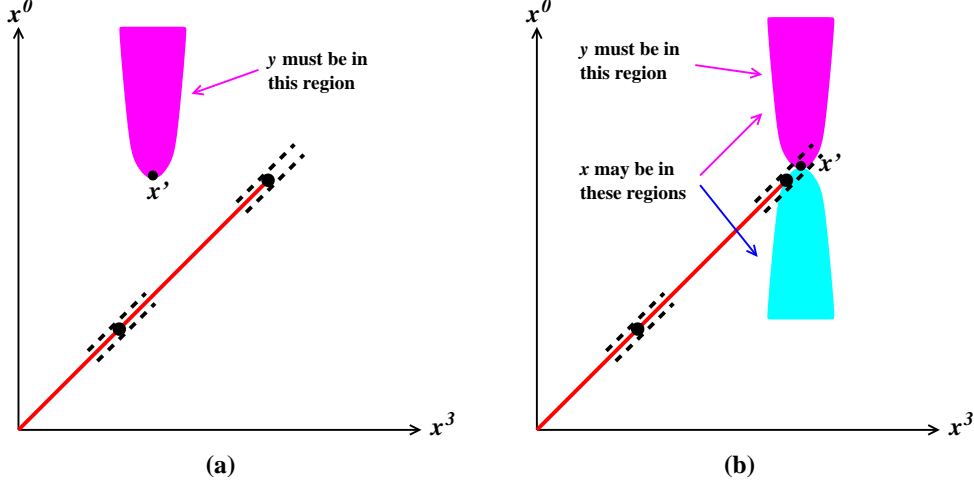


FIG. 18: Restrictions on where the measurement points x and y can be for diagram (c-1) in the cases where the bulk point x' of fig. 17 is (a) far from or (b) near the $x^0 \simeq x^3$ light cone. In the first case, x' cannot be below the lightcone because of causality constraints.

$\frac{1}{2}\langle\{\bar{\Sigma}(x^3), \bar{\Sigma}(y^3)\}\rangle$, of section IID2 with only diagram (a-1). But the causality properties of diagram (a-1) are such that the reasons for carefully defining the refined correlator no longer apply. So, restricting attention to (a-1), there is no reason not to compute the original, simpler correlator $\frac{1}{2}\langle\{\hat{\Theta}(x), \hat{\Theta}(y)\}\rangle$, or its time-integrated version $\frac{1}{2}\langle\{\hat{\Sigma}_{\Theta}(x^0=\infty, \mathbf{x}), \hat{\Sigma}_{\Theta}(y^0=\infty, \mathbf{y})\}\rangle$. That is, we will compute (2.35) with the “relevant diagrams” being (a-1).

IV. THE BULK-TO-BULK CORRELATOR $G_{\text{rr}}^{(5)}$

In order to evaluate diagram (a-1) of fig. 13, we will need the bulk-to-bulk correlator $G_{\text{rr}}^{(5)}$ associated with the internal line of that diagram. (The superscript is a reminder that this is the 5-dimensional bulk correlator and not the 4-dimensional boundary correlator.) When evaluating correlators of the time-integrated charge deposition $\hat{\Sigma}_{\Theta}(x^0=\infty, \mathbf{x})$, we will turn out to need only the case where the two bulk points in diagram (a-1) are at very large times. At very large times, the 5-dimensional excitation created by the source has fallen in the 5th dimension, so that it is localized very near the horizon. In consequence, we will really only need the bulk-to-bulk correlator $G_{\text{rr}}^{(5)}$ between near-horizon points.

In section IV A below, we give a general discussion of how bulk-to-bulk propagators such as $G_{\text{rr}}^{(5)}$ can be computed in terms of more familiar bulk-to-boundary propagators \mathcal{G} . We then specialize in section IV B to the case where both bulk points lie very near the horizon.

A. General case

For diagram (a-1) of fig. 13, we are interested in bulk-to-bulk propagators for a transversely-polarized bulk gauge field A_{\perp} that is dual to the transversely-polarized R-charge current operator j_{\perp} . The generalization to other cases is relatively straightforward.

In particular, in this section we will simultaneously treat the case of a bulk scalar field, which does not require adding any additional indices or other complications of notation and which is relevant to our discussion of $e_{\text{jet}} \gg 1$ in Appendix A.

1. *Bulk-to-bulk* $G_{\text{R}}^{(5)}$

We start by looking at the retarded bulk-to-bulk propagator $G_{\text{R}}^{(5)}$ from one bulk point $X_1 = (x_1, u_1)$ to another $X_2 = (x_2, u_2)$. Note that x_1 and x_2 label 4-positions of bulk points in this discussion and are not the source points we have labeled x_1 and x_2 previously. Let q be the Fourier conjugate of $x_2 - x_1$. We will verify in a moment that $G_{\text{R}}^{(5)}$ can be written in terms of bulk-to-boundary propagators as

$$G_{\text{R}}^{(5)}(u_1; u_2, q) \equiv G_{\text{ar}}^{(5)}(u_1; u_2, q) = \frac{\mathcal{N}_{\text{G}}}{W_{\text{RA}}(q)} \mathcal{G}_{\text{R}}(u_>; q) [\mathcal{G}_{\text{R}}(u_<; q) - \mathcal{G}_{\text{A}}(u_<; q)], \quad (4.1)$$

where $W_{\text{RA}}(q)$ is the Wronskian (to be made explicit in a moment), $u_< \equiv \min(u_1, u_2)$, and $u_> \equiv \max(u_1, u_2)$. The overall normalization \mathcal{N}_{G} comes from the normalization of the kinetic term in the 5-dimensional Lagrangian. For gauge fields, we take $\mathcal{L}_{\text{kin}} = -\frac{1}{4}(g_{\text{SG}}^2 R)^{-1} F^{IJa} F_{IJ}^a$ and correspondingly

$$\mathcal{N}_{\text{G}} = g_{\text{SG}}^2 R, \quad (4.2)$$

where R is the AdS radius and $g_{\text{SG}} = 4\pi/N_c$ [29, 30]. For scalars, $\mathcal{L}_{\text{kin}} = -(g_{\text{SG}}^2 R^3)^{-1} (\partial_I \phi) g^{IJ} (\partial_J \phi)$ and $\mathcal{N}_{\text{G}} = g_{\text{SG}}^2 R^3/2$.

Let's now check that the propagator (4.1) satisfies the equation of motion with a source term at (x_1, u_1) :

$$\frac{1}{\mathcal{N}_{\text{G}}} \left[\partial_I (\sqrt{-g} g^{IJ} \lambda \partial_J) - \sqrt{-g} m^2 \right] G_{\text{R}}^{(5)}(X_1; X) = \delta^{(5)}(X - X_1), \quad (4.3)$$

where

$$\lambda \equiv \begin{cases} g^{\perp\perp}, & \text{transverse gauge field } A_{\perp}; \\ 1, & \text{scalar field } \phi, \end{cases} \quad (4.4)$$

and $m = 0$ in the gauge field case. In 4-momentum space, this is

$$\frac{1}{\mathcal{N}_{\text{G}}} \left[\partial_5 (\sqrt{-g} g^{55} \lambda \partial_5) - \sqrt{-g} (\lambda q_{\mu} g^{\mu\nu} q_{\nu} + m^2) \right] G_{\text{R}}^{(5)}(u_1; u, q) = \delta(u - u_1). \quad (4.5)$$

From the fact that the bulk-to-boundary propagators satisfy the homogeneous equation

$$\frac{1}{\mathcal{N}_{\text{G}}} \left[\partial_5 (\sqrt{-g} g^{55} \lambda \partial_5) - \sqrt{-g} (\lambda q_{\mu} g^{\mu\nu} q_{\nu} + m^2) \right] \mathcal{G}(u; q) = 0, \quad (4.6)$$

one can verify that (4.1) satisfies (4.5) provided $W_{\text{RA}}(q)$ is the Wronskian

$$W_{\text{RA}} = \sqrt{-g} g^{55} \lambda (\mathcal{G}_{\text{R}} \overleftrightarrow{\partial}_5 \mathcal{G}_{\text{A}}), \quad (4.7)$$

which is independent of u . Here, $\overleftrightarrow{\partial}$ is defined by $f \overleftrightarrow{\partial} g \equiv f \partial g - (\partial f) g$.

For the bulk-to-boundary propagator $\mathcal{G}(u; q)$, our convention is that q is the momentum conjugate to the boundary point. For the bulk-to-bulk correlator $G_{\text{R}}^{(5)}(u_1; u_2, q)$, the convention is that q is associated with the bulk point at u_2 , which we take to be the later-time

point in defining the retarded correlator. Eq. (4.1) gives a *retarded* bulk-to-bulk correlator because it is analytic in the upper-half q^0 plane since (i) $\mathcal{G}_R(u; q)$ has this property and (ii) the poles in $\mathcal{G}_A(u_<; q)$ cancel the corresponding poles in the denominator W_{RA} .

Finally, bulk-to-bulk propagators should satisfy the correct boundary condition at the boundary, which is that the boundary is fixed and so fluctuation fields (such as ϕ and A_\perp) should vanish there in this context. That is, $G^{(5)}(u_1; u_2, q)$ should vanish for u_1 or u_2 zero. This is easy to see for (4.1) in the case of A_\perp or massless scalar fields, since the bulk-to-boundary propagators are then normalized to 1 at the boundary, so that $\mathcal{G}_A(0; q) - \mathcal{G}_R(0; q) = 0$. Eq. (4.1) also satisfies the boundary condition in the massive scalar case, but there one must take care to regulate the boundary.

2. Bulk-to-bulk $G_A^{(5)}$

The advanced bulk-to-bulk propagator is similarly

$$G_A^{(5)}(u_1; u_2, q) \equiv G_{ra}^{(5)}(u_1; u_2, q) = \frac{\mathcal{N}_G}{W_{RA}(q)} \mathcal{G}_A(u_>; q) [\mathcal{G}_R(u_<; q) - \mathcal{G}_A(u_<; q)]. \quad (4.8)$$

3. Bulk-to-bulk $G_{rr}^{(5)}$

Applying (3.3) then produces

$$\begin{aligned} G_{rr}^{(5)}(u_1; u_2, q) &= \text{cth}(\frac{1}{2}\beta\omega) [G_R^{(5)}(u; q) - G_A^{(5)}(u; q)] \\ &= \text{cth}(\frac{1}{2}\beta\omega) \frac{\mathcal{N}_G}{W_{RA}(q)} [\mathcal{G}_R(u_1; q) - \mathcal{G}_A(u_1; q)] [\mathcal{G}_R(u_2; q) - \mathcal{G}_A(u_2; q)]. \end{aligned} \quad (4.9)$$

B. Near-horizon case

Here and throughout the rest of this paper, we will work in units where $2\pi T=1$ and specialize to the choice of 5th dimension coordinate u with metric (2.1).

1. Near-horizon bulk-to-boundary propagator

Near the horizon, the general solution to the homogeneous equation of motion (4.6) with the boundary conditions appropriate to \mathcal{G}_R can be expanded in powers of $1-u$ as

$$\mathcal{G}_R(u; q) = b(q) (1-u)^{-i\omega/2} [1 + O(1-u)]. \quad (4.10)$$

We will not need the exact solution away from the horizon.¹⁴ All of its complexity is summarized here in the factor $b(q)$, which is determined by the normalization condition for

¹⁴ As an example, for the case of A_\perp , the exact solution is given by replacing $[1 + O(1-u)]$ in (4.10) by $[\frac{1}{2}(1+u)]^{\omega/2} \text{Hl}(2, q^2 - \frac{i}{2}\omega^2 + \frac{1-i}{2}\omega; \frac{1-i}{2}\omega, \frac{1-i}{2}\omega + 1, 1-i\omega, 0; 1-u)$, where Hl is a Heun function as defined in ref. [31].

\mathcal{G}_R on the boundary (e.g. $\mathcal{G}_R(0; q) = 1$ for A_\perp and massless scalar fields). The answer to our question of whether jet charge deposition is correlated over relatively large distances will turn out not to depend on the details of $b(q)$ — all that will matter are some simple analytic properties of $b(q)$. Since \mathcal{G}_R is a retarded propagator, $b(q)$ must be analytic in the upper-half complex frequency plane. Because $[\mathcal{G}_R(u; -q)]^* = \mathcal{G}_R(u; q)$ for real q , (4.10) also gives the important relation

$$b(-q) = b^*(q) \quad \text{for real } q. \quad (4.11)$$

It will be convenient to change variables from u to

$$\tau \simeq -\frac{1}{2} \ln(1 - u). \quad (4.12)$$

The \simeq indicates that the details of the definition will not matter with regard to sub-leading corrections as $u \rightarrow 1$. Physically, τ represents the time (as measured by an asymptotic observer) for the a wave in the bulk to propagate from near the boundary to the near-horizon position $u \simeq 1$, and details such as initial conditions or phase vs. group velocity only affect sub-logarithmic corrections to (4.12). In terms of τ , (4.10) becomes

$$\mathcal{G}_\perp^R(u; q) = b(q) e^{i\omega\tau} [1 + O(e^{-2\tau})]. \quad (4.13)$$

2. Near-horizon bulk-to-bulk $G_R^{(5)}$

We now turn to $G_R^{(5)}$ as given by (4.1). For simplicity of presentation, we will specialize here to the case of the A_\perp propagator and quote the scalar case at the end. We first need the Wronskian (4.7). Since the Wronskian is u -independent, we can evaluate (4.7) at any u , and it is most convenient to evaluate it in the horizon limit $u \rightarrow 1$. Using (4.10) and its conjugate

$$\mathcal{G}_A(u; q) = \mathcal{G}_R(u; -q) = b(-q) (1 - u)^{i\omega/2} [1 + O(1 - u)], \quad (4.14)$$

together with

$$\sqrt{-g} g^{55} g^{\perp\perp} = \frac{1}{2} Rf \rightarrow R(1 - u), \quad (4.15)$$

we get

$$W_{RA} = -iR\omega b(q) b(-q), \quad (4.16)$$

which for real q is $W_{RA} = -iR\omega |b(q)|^2$. Combining (4.16) with (4.1) and (4.13), the near-horizon limit of the retarded bulk-to-bulk propagator is

$$\begin{aligned} iG_R^{(5)}(\tau_1; \tau_2, q) &\simeq \frac{g_{\text{SG}}^2}{\omega} e^{i\omega\tau_2} [-e^{i\delta(q)} e^{i\omega\tau_1} + e^{-i\omega\tau_1}] \\ &= \frac{g_{\text{SG}}^2}{\omega} [-e^{i\delta(q)} e^{i\omega(\tau_2 + \tau_1)} + e^{i\omega|\tau_2 - \tau_1|}], \end{aligned} \quad (4.17)$$

where

$$e^{i\delta(q)} \equiv \frac{b(q)}{b(-q)}. \quad (4.18)$$

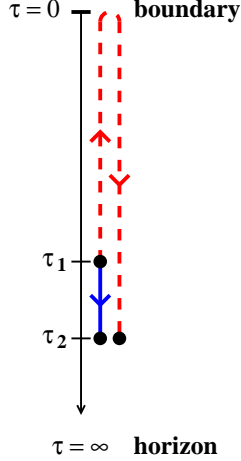


FIG. 19: Schematic representation of the two contributions to the near-horizon bulk-to-bulk retarded propagator (4.17).

For real q , the phase $\delta(q)$ is real. At poles of $G_R^{(5)}$ in the lower-half complex frequency plane, δ becomes $-i\infty$. The right-hand side of (4.17) is finite as $\omega \rightarrow 0$ because¹⁵

$$\delta(\omega, \mathbf{q}) \rightarrow 0 \quad \text{linearly as} \quad \omega \rightarrow 0. \quad (4.19)$$

For scalar fields, the result is a factor of 2 larger than (4.17).

To understand the physical interpretation of the two terms on the right-hand side of (4.17), consider the metric (2.1) in the near-horizon limit,

$$ds^2 \simeq \frac{R^2}{4} [-f dt^2 + d\mathbf{x}^2 + f d\tau^2] \quad (4.20)$$

with $f \simeq 2(1-u) \simeq 2e^{-2\tau}$. Note that points with different \mathbf{x} are far apart compared to points with different t or τ . Because of this, the \mathbf{x} motion decouples. More concretely, the equation of motion (4.5) satisfied by the A_\perp propagator is

$$(\partial_\tau^2 + \omega^2) G_R^{(5)}(\tau_1; \tau, q) \simeq 2g_{\text{SG}}^2 \delta(\tau - \tau_1) \quad (4.21)$$

in the near-horizon limit for fixed q . This looks similar to a flat-space problem in one space-time dimension, where the Green function would be proportional to $(i\omega)^{-1} e^{i\omega|\Delta\tau|}$. Compare to (4.17). The second term on the right-hand side of (4.17) corresponds to a signal that travels directly from τ_1 to τ_2 , corresponding to a distance $|\tau_2 - \tau_1|$ in τ . The first term, in contrast, corresponds to a signal that travels from τ_1 to the boundary $\tau=0$ and then reflects back to τ_2 , traveling a total τ -distance proportional to $\tau_2 + \tau_1$. $\delta(q)$ represents the phase shift that the wave picks up traveling through the region far from the horizon, where the dynamics becomes more complicated than the simple asymptotic behavior (4.21). The relative minus sign between the two terms is because the wave flips when it reflects from the boundary due to the boundary condition that the Green function vanish at the horizon. The two contributions to the right-hand side of (4.17) are depicted schematically in fig. 19.

¹⁵ Presumably there is some simple way to understand (4.19), but we just checked it numerically.

3. Near-horizon bulk-to-bulk $G_{\text{rr}}^{(5)}$

Applying the same results to the formula (4.9) for $G_{\text{rr}}^{(5)}$ gives, in units where $2\pi T = 1$,

$$\begin{aligned} iG_{\text{rr}}^{(5)}(u_1; u_2, q) &\simeq g_{\text{SG}}^2 \frac{\text{cth}(\pi\omega)}{\omega} (e^{i\omega\tau_1} - e^{-i\delta(q)} e^{-i\omega\tau_1}) (e^{-i\omega\tau_2} - e^{i\delta(q)} e^{i\omega\tau_2}) \\ &= 2g_{\text{SG}}^2 \frac{\text{cth}(\pi\omega)}{\omega} \left[-\cos(\omega(\tau_2 + \tau_1) + \delta(q)) + \cos(\omega(\tau_2 - \tau_1)) \right]. \end{aligned} \quad (4.22)$$

Note that the $\omega \rightarrow 0$ limit is finite because of (4.19).

The second term in (4.22) is independent of \mathbf{q} and so is a δ -function $\delta^{(3)}(\mathbf{x}_1 - \mathbf{x}_2)$ in 3-position space. This locality is a consequence of the fact that \mathbf{x} motion is suppressed near the horizon. In contrast, the first term does depend on \mathbf{q} through the phase $\delta(q)$ and so can produce non-local correlations in \mathbf{x} . This non-locality arises because the phase δ appears in contributions like the dashed line in fig. 19, corresponding to propagation away from the horizon, so that 3-space dynamics are then nontrivial, bouncing off of the boundary, and then propagating back to near the horizon. We will see that only the second term in (4.22) contributes significantly to charge deposition correlations for high-energy jets, and the locality of that term will be responsible for the locality of the charge deposition correlation.

In Appendix B, we show how to relate our result (4.22) to expressions derived for bulk-to-bulk G_{rr} by Caron-Huot, Chesler, and Teaney [10] in the context of fluctuations of a classical string.

V. CALCULATING THE CORRELATOR

A. Starting formula

We are now finally ready to calculate the contribution of diagram (a-1) of fig. 13 to our correlator. In our application, only the standard Yang-Mills 3-point vertices contribute to this diagram: the contributions from the Chern-Simons term in the SUGRA Lagrangian vanish because the $\text{SU}(4)$ group factor $d^{\pm 3e} \equiv 2 \text{tr}[\{T^\pm, T^3\}T^e]$ that would be associated with a Chern-Simons 3-point vertex vanishes.

To save space, we will henceforth abbreviate $\langle \frac{1}{2}\{j^{(3)\mu}(x), j^{(3)\nu}(y)\} \rangle$ as $\langle \frac{1}{2}\{j^\mu, j^\nu\} \rangle$. Plugging the source (2.5b) into the relationship (3.11) between $\langle \frac{1}{2}\{j^\mu, j^\nu\} \rangle$ and the 4-point equilibrium correlator G_{arr} , and expressing G_{arr} in momentum space, gives

$$\begin{aligned} \Delta \langle \frac{1}{2}\{j^\mu, j^\nu\} \rangle &= i \frac{\mathcal{N}_A^2}{2} \int_{QQ'Q_1Q_2} \bar{\varepsilon}_\alpha \bar{\varepsilon}_\beta G_{\text{arr}}^{(-+33)\alpha\beta\mu\nu}(Q_1, Q_2; Q, Q') \tilde{\Lambda}_L^*(Q_1 - \bar{k}) \tilde{\Lambda}_L^*(Q_2 + \bar{k}) \\ &\quad \times e^{iQ \cdot x} e^{iQ' \cdot y} (2\pi)^4 \delta^{(4)}(Q + Q' + Q_1 + Q_2). \end{aligned} \quad (5.1)$$

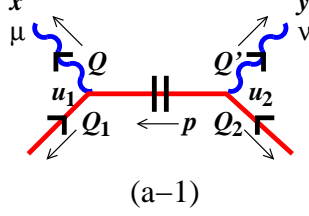


FIG. 20: Naming conventions for momenta assignments to diagram (a-1).

Labeling momenta as in fig. 20, diagram (a-1) plus its permutations gives

$$\begin{aligned}
[\bar{\varepsilon}_\alpha \bar{\varepsilon}_\beta (G_{\text{arr}})^{(-+33)\alpha\beta\mu\nu}]_{(a-1)} &= i f^{-e3} f^{e+3} \\
&\times \frac{i(-p-Q_1)_\rho}{g_{\text{SG}}^2 R} \int du_1 (\sqrt{-g} g^{\perp\perp} g^{\rho\sigma})_1 \mathcal{G}_\perp^A(u_1; Q_1) \mathcal{G}_\sigma^{\text{R}\mu}(u_1; Q) \\
&\times \frac{i(Q_2-p)_\xi}{g_{\text{SG}}^2 R} \int du_2 (\sqrt{-g} g^{\perp\perp} g^{\xi\tau})_2 \mathcal{G}_\perp^A(u_2; Q_2) \mathcal{G}_\tau^{\text{R}\nu}(u_2; Q') \\
&\times i G_{\text{rr}\perp}^{(5)}(u_1; u_2, -p) \Big|_{p=Q_1+Q_2=-(Q_2+Q')} \\
&+ \{Q, \mu \leftrightarrow Q', \nu\}.
\end{aligned} \tag{5.2}$$

The group factors are $f^{-e3} f^{e+3} = -2$. In Appendix C, we show that these formulas give a simple and easily predictable result for $\Delta\langle\frac{1}{2}\{j^\mu, j^\nu\}\rangle$ in the $T=0$ case. But here we focus on finite temperature and the contribution of diagram (a-1) to $\frac{1}{2}\langle\{\hat{\Sigma}_\Theta(x^0=\infty, \mathbf{x}), \hat{\Sigma}_\Theta(y^0=\infty, \mathbf{y})\}\rangle$, which we will abbreviate as $\frac{1}{2}\langle\{\hat{\Sigma}_\Theta, \hat{\Sigma}_\Theta\}\rangle$ in the following.

From the definitions (2.16b) and (2.15) of $\hat{\Sigma}_\Theta$ and $\hat{\Theta}$, replacing j^μ and j^ν by $\hat{\Sigma}_\Theta$ in (5.1) is equivalent to replacing

$$\mathcal{G}_\sigma^{\text{R}\mu}(u_1; Q) \rightarrow \frac{iQ^0 - DQ^2}{iQ^0} \mathcal{G}_\sigma^{\text{R}0}(u_1; Q) \tag{5.3}$$

and similarly for $\mathcal{G}_\tau^{\text{R}\nu}(u_2; Q')$ in (5.2). Note that the R-charge diffusion constant (2.14) is $D=1$ in our units $2\pi T=1$. As reviewed earlier, our measurements do not need to resolve scales as small as $1/T$ in order to study jet stopping, and so we may make small-momentum approximations for the momenta Q and Q' conjugate to the measurement points x and y . In previous work [3], we discussed how the corresponding low-momentum bulk-to-boundary propagators are

$$\mathcal{G}_0^{\text{R}0}(\omega, k) \simeq \frac{i\omega}{i\omega - k^2} - \frac{k^2}{i\omega - k^2} (1-u)^{1-i\omega/2}, \tag{5.4}$$

$$\mathcal{G}_3^{\text{R}0}(\omega, k) \simeq -\frac{ik}{i\omega - k^2} + \frac{ik}{i\omega - k^2} (1-u)^{-i\omega/2}. \tag{5.5}$$

We also showed that for the purposes of computing $\langle\Sigma_\Theta(x^0=\infty, \mathbf{x})\rangle$, only near-horizon values

of u were important and that in that limit one could replace¹⁶

$$\mathcal{G}_0^{\text{R}0}(\omega, k) \simeq \frac{i\omega}{i\omega - k^2} \quad (5.6a)$$

and ignore $\mathcal{G}_3^{\text{R}0}$ altogether in the calculation:

$$\mathcal{G}_3^{\text{R}0}(\omega, k) \simeq 0. \quad (5.6b)$$

The same will happen in computing the correlation of $\hat{\Sigma}_\Theta$. Using (5.6) in (5.3), we see that replacing the j 's by $\hat{\Sigma}_\Theta$'s in (5.1) amounts to replacing

$$\mathcal{G}_\sigma^{\text{R}\mu}(u_1; Q) \rightarrow \delta_\sigma^0 \quad \text{and} \quad \mathcal{G}_\tau^{\text{R}\nu}(u_2; Q') \rightarrow \delta_\tau^0 \quad (5.7)$$

in (5.2). Putting everything together and using

$$\sqrt{-g} g^{00} g^{\perp\perp} = \frac{R}{2uf} \quad (5.8)$$

gives

$$\begin{aligned} \langle \frac{1}{2} \{ \hat{\Sigma}_\Theta, \hat{\Sigma}_\Theta \} \rangle_{(a-1)} &\simeq \frac{\mathcal{N}_A^2}{4g_{\text{SG}}^4} \int \frac{du_1}{u_1 f_1} \frac{du_2}{u_2 f_2} \mathcal{A}^*(x, u_1) \overleftrightarrow{\partial}_{x^0} iG_{\text{rr}\perp}^{(5)}(x, u_1; y, u_2) \overleftrightarrow{\partial}_{y^0} \mathcal{A}(y, u_2) \\ &\quad + \{x \leftrightarrow y\}, \end{aligned} \quad (5.9)$$

where

$$\mathcal{A}(x, u) \equiv \int_q \mathcal{G}_\perp^{\text{R}}(u; q) \tilde{\Lambda}_L(q - \bar{k}) e^{iq \cdot x} \quad (5.10)$$

describes the bulk vector field created by the source and

$$\mathcal{A}^*(x, u) = \int_q \mathcal{G}_\perp^{\text{A}}(u; q) \tilde{\Lambda}_L^*(q - \bar{k}) e^{-iq \cdot x}. \quad (5.11)$$

For comparison, the corresponding formula for $\langle \hat{\Sigma}_\Theta \rangle$ is [3]

$$\langle \hat{\Sigma}_\Theta \rangle \simeq \frac{\mathcal{N}_A^2}{g_{\text{SG}}^2} \int \frac{du}{uf} \mathcal{A}^*(x, u) i\overleftrightarrow{\partial}_{x^0} \mathcal{A}(x, u). \quad (5.12)$$

At this point, it is useful to think again in momentum space, where the operators $\overleftrightarrow{\partial}_{x^0}$ and $\overleftrightarrow{\partial}_{y^0}$ in (5.9) become the $-i(-p - Q_1)_0$ and $-i(Q_2 - p)_0$ factors in (5.2) respectively. As mentioned earlier, our resolution requirements permit approximating Q and Q' as small, in which case these factors may be approximated by $2i(Q_1)_0$ and $-2i(Q_2)_0$. Because of the source factors Λ_L in (5.1), our calculation only gets contributions from $(Q_1)_0 \simeq -E$ and $(Q_2)_0 \simeq E$. The upshot is that the two operators $\overleftrightarrow{\partial}_0$ in (5.9) may each be replaced by $-2iE$:

$$\langle \frac{1}{2} \{ \hat{\Sigma}_\Theta, \hat{\Sigma}_\Theta \} \rangle_{(a-1)} \simeq -2E^2 \frac{\mathcal{N}_A^2}{g_{\text{SG}}^4} \text{Re} \int \frac{du_1}{u_1 f_1} \frac{du_2}{u_2 f_2} \mathcal{A}^*(x, u_1) iG_{\text{rr}\perp}^{(5)}(x, u_1; y, u_2) \mathcal{A}(y, u_2). \quad (5.13)$$

¹⁶ See specifically the discussion in sections IV.A.1 and IV.G of ref. [3].

B. Factorizing $G_{\text{rr}}^{(5)}$

Let us return to momentum space for $G_{\text{rr}}^{(5)}$:

$$\begin{aligned} \langle \frac{1}{2} \{ \hat{\Sigma}_{\Theta}, \hat{\Sigma}_{\Theta} \} \rangle_{(a-1)} &\simeq \\ &- 2E^2 \frac{\mathcal{N}_A^2}{g_{\text{SG}}^4} \text{Re} \int_p \int \frac{du_1}{u_1 f_1} \frac{du_2}{u_2 f_2} \mathcal{A}^*(x, u_1) e^{ip \cdot x} i G_{\text{rr}\perp}^{(5)}(u_1; u_2, -p) e^{-ip \cdot y} \mathcal{A}(y, u_2). \end{aligned} \quad (5.14)$$

Using the general formula (4.9) for $G_{\text{rr}}^{(5)}$ and the result (4.16) for W_{RA} , the u_1 and u_2 integrals factorize as

$$\langle \frac{1}{2} \{ \hat{\Sigma}_{\Theta}, \hat{\Sigma}_{\Theta} \} \rangle_{(a-1)} \simeq 2E^2 \frac{\mathcal{N}_A^2}{g_{\text{SG}}^2} \text{Re} \int_p \frac{\text{cth}(\pi p^0)}{p^0 |b(p)|^2} \mathcal{J}^*(p, x) \mathcal{J}(p, y), \quad (5.15)$$

where

$$\begin{aligned} \mathcal{J}(p, x) &\equiv \int \frac{du}{uf} [\mathcal{G}_{\perp}^{\text{R}}(u; p) - \mathcal{G}_{\perp}^{\text{A}}(u; p)] e^{-ip \cdot x} \mathcal{A}(x, u) \\ &= \int_q \tilde{\Lambda}_L(q - \bar{k}) e^{i(q-p) \cdot x} \int \frac{du}{uf} \mathcal{G}_{\perp}^{\text{R}}(u; q) [\mathcal{G}_{\perp}^{\text{R}}(u; p) - \mathcal{G}_{\perp}^{\text{A}}(u; p)]. \end{aligned} \quad (5.16)$$

C. The u integral

We now evaluate the u integral in (5.16),

$$I_{qp} \equiv \int \frac{du}{uf} \mathcal{G}_{\perp}^{\text{R}}(u; q) [\mathcal{G}_{\perp}^{\text{R}}(u; p) - \mathcal{G}_{\perp}^{\text{A}}(u; p)]. \quad (5.17)$$

Consider the near-horizon (large τ) approximation to the integrand. Using (4.13) for $\mathcal{G}_{\perp}^{\text{R}}$ and using $du/uf \simeq d\tau$,¹⁷

$$I_{qp} \simeq b(q) \int_0^{\infty} d\tau e^{iq^0 \tau} [b(p) e^{ip^0 \tau} - b^*(p) e^{-ip^0 \tau}]. \quad (5.18)$$

Recall that q^0 is really $q^0 + i\epsilon$ because of the retarded prescription on q . The integral is then

$$I_{qp} \simeq ib(q) \left[\frac{b(p)}{q^0 + p^0 + i\epsilon} - \frac{b^*(p)}{q^0 - p^0 + i\epsilon} \right]. \quad (5.19)$$

Why is it okay to make the near-horizon approximation for the bulk-to-bulk propagator? We are interested in evaluating the correlator (5.14) of $\hat{\Sigma}_{\Theta}$'s at $x^0, y^0 \rightarrow \infty$. In this limit, $\mathcal{A}(x, u_1)$ and $\mathcal{A}(y, u_2)$ are exponentially suppressed everywhere except very close to the horizon ($\tau \gg 1$) [3].¹⁸

¹⁷ We will consider only real values of p (but complex values of q) in what follows, and so $b(-p)$ and $b^*(p)$ are interchangeable as in (4.11).

¹⁸ We can see this in detail from the exponential tail derived in our previous work [3] for large $X^+ \equiv x^+ - \tau(u)$:

$$\mathcal{A}(x, u) \simeq i e^{iE[x^- + \tau(u)]} \text{Res} \left[\bar{\mathcal{G}}_{\perp}^{\text{R}}(u; q_+^{(1)}) \Lambda_L^{(2)}(q_+^{(1)}; x^- + \tau(u)) e^{-\text{Im}(q_+^{(1)}) X^+} \right].$$

Large x^0 for fixed x^3 corresponds to large $-x^-$ and x^+ . From the $x^- + \tau$ argument of Λ_L , we therefore get exponential suppression unless $\tau \simeq -x^-$ is also large. In this case, $X^+ \simeq 2x^3$.

Note from (4.13) that corrections to the near-horizon limit formulas for our propagators are suppressed by $e^{-2\tau}$, and so these corrections vanish in the large-time limit of interest.

D. The q^0 integral

Putting the result (5.19) for the u integral back into eq. (5.16) for \mathcal{J} gives

$$\mathcal{J}(p, x) = i b(p) \int_q b(q) \tilde{\Lambda}_L(q - \bar{k}) \frac{e^{i(q-p)\cdot x}}{q^0 + p^0 + i\epsilon} - i b^*(p) \int_q b(q) \tilde{\Lambda}_L(q - \bar{k}) \frac{e^{i(q-p)\cdot x}}{q^0 - p^0 + i\epsilon}. \quad (5.20)$$

Now do the q^0 integral by closing the integral in the lower half-plane,¹⁹ and look at the contribution from picking up the explicit poles above:

$$\begin{aligned} \mathcal{J}(p, x) \simeq e^{2ip^0 x^0} b(p) \int_{\mathbf{q}} b(-p^0, \mathbf{q}) \tilde{\Lambda}_L(-p^0 - E, \mathbf{q} - \bar{\mathbf{k}}) e^{i(\mathbf{q}-\mathbf{p})\cdot\mathbf{x}} \\ - b^*(p) \int_{\mathbf{q}} b(p^0, \mathbf{q}) \tilde{\Lambda}_L(p^0 - E, \mathbf{q} - \bar{\mathbf{k}}) e^{i(\mathbf{q}-\mathbf{p})\cdot\mathbf{x}}. \end{aligned} \quad (5.21)$$

Before we use this expression, we should consider what other singularities contribute to the integral. In particular, $b(q)$ has poles in the lower-half q^0 plane, corresponding to quasinormal modes. When evaluated at these poles, the $e^{-iq^0 x^0}$ term in the integrand will give a suppression factor of order

$$e^{x^0 \text{Im } q_{\text{pole}}^0}. \quad (5.22)$$

(Keep in mind that $\text{Im } q_{\text{pole}}^0$ is negative.) But we are interested specifically in the $x^0 \rightarrow \infty$ limit for evaluating $\hat{\Sigma}_\Theta$, and so these contributions will vanish. Because $\tilde{\Lambda}_L$ only has support for $q_- \simeq E$, where the poles in q_+ have imaginary parts of $O(E^{-1/3})$ [3], the relevant poles in $q^0 = q_- - q_+$ have imaginary parts of $-O(E^{-1/3})$.

Because of the support of the envelope factor $\tilde{\Lambda}_L$ in the first term of (5.21), the $e^{2ip^0 x^0}$ phase factor in that term has $p^0 \simeq E$ and so is highly oscillatory. Remember that we are only trying to resolve distance and time scales of the observables on scales large compared to $1/T$. If we smear out our observables $\hat{\Sigma}_\Theta(x)$ and $\hat{\Sigma}_\Theta(y)$ over such scales, then the contribution of such a highly-oscillating phase will be smeared away.²⁰ As a result, we may drop the first

¹⁹ Technically, some care should be taken here because of the behavior of Λ_L in the complex frequency plane. Really, one should take care to route the closing piece of the contour through regions of the complex plane where the integrand is exponentially suppressed. See Appendix E of ref. [3] for related discussion (though there the contour is different and serves a different purpose).

²⁰ More specifically, suppose we replace $\hat{\Sigma}_\Theta(x)$ by

$$[\hat{\Sigma}_\Theta(x)]_{\text{smeared}} \equiv \int d^4(\Delta x) \hat{\Sigma}_\Theta(x + \Delta x) \frac{e^{-(\Delta x^0)^2/\ell_{\text{smear}}^2} e^{-|\Delta \mathbf{x}|^2/\ell_{\text{smear}}^2}}{\pi \ell_{\text{smear}}^2}$$

as discussed in sec. II B of ref. [3], where the smearing distance ℓ_{smear} is chosen large compared to microscopic scales such as $1/E$ and $1/T$ but small compared to the scales we're interested in resolving, such as stopping distances. If one applies this procedure to something that behaves like $\exp(i2Ex^0)$, then one obtains an exponentially small result.

term of (5.21) and simply write

$$\mathcal{J}(p, x) \simeq -b^*(p) \int_{\mathbf{q}} b(p^0, \mathbf{q}) \tilde{\Lambda}_L(p^0 - E, \mathbf{q} - \bar{\mathbf{k}}) e^{i(\mathbf{q}-p)\cdot\mathbf{x}}. \quad (5.23)$$

E. Assembling the pieces

Now use the expression (5.23) for \mathcal{J} in the correlator (5.15) of $\hat{\Sigma}_\Theta$'s:

$$\begin{aligned} \langle \frac{1}{2} \{ \hat{\Sigma}_\Theta, \hat{\Sigma}_\Theta \} \rangle_{(a-1)} &\simeq 2E^2 \frac{\mathcal{N}_A^2}{g_{\text{SG}}^2} \text{Re} \int_p \frac{\text{cth}(\pi p^0)}{p^0} e^{i\mathbf{p}\cdot(\mathbf{x}-\mathbf{y})} \int_{\mathbf{q}\mathbf{q}'} e^{-i\mathbf{q}\cdot\mathbf{x}} e^{-i\mathbf{q}'\cdot\mathbf{y}} \\ &\times b^*(p^0, \mathbf{q}) b(p^0, \mathbf{q}') \tilde{\Lambda}_L^*(p^0 - E, \mathbf{q} - \bar{\mathbf{k}}) \tilde{\Lambda}_L(p^0 - E, \mathbf{q}' - \bar{\mathbf{k}}). \end{aligned} \quad (5.24)$$

Now note that the \mathbf{p} integral just gives $\delta^{(3)}(\mathbf{x} - \mathbf{y})$:

$$\begin{aligned} \langle \frac{1}{2} \{ \hat{\Sigma}_\Theta, \hat{\Sigma}_\Theta \} \rangle_{(a-1)} &\simeq 2E^2 \frac{\mathcal{N}_A^2}{g_{\text{SG}}^2} \delta^{(3)}(\mathbf{x} - \mathbf{y}) \text{Re} \int_{p^0} \frac{\text{cth}(\pi p^0)}{p^0} \int_{\mathbf{q}\mathbf{q}'} e^{-i\mathbf{q}\cdot\mathbf{x}} e^{-i\mathbf{q}'\cdot\mathbf{y}} \\ &\times b^*(p^0, \mathbf{q}) b(p^0, \mathbf{q}') \tilde{\Lambda}_L^*(p^0 - E, \mathbf{q} - \bar{\mathbf{k}}) \tilde{\Lambda}_L(p^0 - E, \mathbf{q}' - \bar{\mathbf{k}}). \end{aligned} \quad (5.25)$$

The right-hand side vanishes for $\mathbf{x} \neq \mathbf{y}$. Recall that throughout we have made approximations that blur our resolution of \mathbf{x} and \mathbf{y} on the scale $1/T$.

And so we have answered the question we set out to answer: For $|\mathbf{x} - \mathbf{y}|$ large compared to $1/T$, the correlation is exponentially small (coming from all the exponentially-small corrections that we dropped throughout).

Acknowledgments

We gratefully acknowledge Chaolun Wu for his role in deriving the Heun function expression in footnote 21. We thank Sangyong Jeon and Derek Teaney for useful conversations. This work was supported, in part, by the U.S. Department of Energy under Grant No. DE-FG02-97ER41027.

Appendix A: Generalization to jets with large R charge

In this appendix, we discuss how the argument in the main text is modified if one uses a source operator with R charge larger than one. For simplicity, we will consider scalar operators. An example is $\text{tr}(X^\Delta)$, where X is any one of the three complex scalar fields in $\mathcal{N}=4$ SYM. This operator has conformal dimension Δ . The R charge J of $\text{tr}(X^\Delta)$ is Δ under a U(1) subgroup of the SU(4) R charge symmetry, which is the subgroup that we will choose for our measurement operators $j^0(x)$ and $j^0(y)$. [That is, it is the U(1) subgroup that corresponds to $\tau^3/2$ in the main text.]

In what follows, we more generally consider taking our source operator to be any scalar BPS operator of conformal dimension Δ and R charge J under a U(1) R symmetry subgroup. In the 5-dimensional bulk these correspond to scalar fluctuations of mass m such that

$$\Delta = \frac{d}{2} + \sqrt{\left(\frac{d}{2}\right)^2 + m^2 R^2}, \quad (\text{A1})$$

where $d=4$ is the number of boundary space-time dimensions. The important property of the bulk-to-boundary scalar propagator is that it takes the form

$$\mathcal{G}_R(u, q) = b(q) (1 - u)^{-i\omega/2} [1 + O(1 - u)] = b(q) e^{i\omega\tau} [1 + O(e^{-2\tau})] \quad (\text{A2})$$

near the horizon, similar to (4.10) and (4.13) but with a different function $b(q)$ than in the transverse gauge boson case. Near the boundary $u=0$ it behaves like

$$\mathcal{G}_R(u, q) \propto u^{(d-\Delta)/2} [1 + O(u)]. \quad (\text{A3})$$

The divergence of the bulk-to-boundary propagator at the horizon for $d > \Delta$ (related to the need to renormalize such operators) will not have any effect on our calculation, which will be controlled by the near-horizon behavior.²¹

In the vicinity of the horizon, the bulk-to-bulk retarded and symmetrized propagators take the form

$$iG_R^{(5)}(\tau_1; \tau_2, q) = 2 \frac{g_{\text{SG}}^2}{\omega} e^{i\omega\tau} [-e^{i\delta(q)} e^{i\omega\tau} + e^{-i\omega\tau}] \quad (\text{A4})$$

$$iG_{\text{rr}}^{(5)}(\tau_1; \tau_2, q) = 4g_{\text{SG}}^2 \frac{\text{cth}(\pi\omega)}{\omega} \left[-\cos(\omega(\tau_2 + \tau_1) + \delta(q)) + \cos(\omega(\tau_2 - \tau_1)) \right], \quad (\text{A5})$$

where, as before, $e^{i\delta(q)} \equiv b(q)/b(-q)$. These formulas differ from the transverse boson case (4.17) and (4.22) by a factor of 2 normalization (and $\delta(q)$ is a different function of q).

For a scalar field with R charge J , the same real-time Witten diagram (a-1) as in the main text gives

$$\begin{aligned} [(G_{\text{aarr}})^{(33)\mu\nu}]_{(a-1)} &= -iJ^2 \\ &\times \frac{2i(-p - Q_1)_\rho}{g_{\text{SG}}^2 R^3} \int du_1 (\sqrt{-g}g^{\rho\sigma})_1 \mathcal{G}_A(Q_1, u_1) \mathcal{G}_\sigma^{\text{R}\mu}(Q, u_1) \\ &\times \frac{2i(Q_2 - p)_\xi}{g_{\text{SG}}^2 R^3} \int du_2 (\sqrt{-g}g^{\xi\tau})_2 \mathcal{G}_A(Q_2, u_2) \mathcal{G}_\tau^{\text{R}\nu}(Q', u_2) \\ &\times iG_{\text{rr}}^{(5)}(u_1; u_2, -p) \Big|_{p=Q_1+Q=-(Q_2+Q')} \\ &+ \{Q, \mu \leftrightarrow Q', \nu\}. \end{aligned} \quad (\text{A6})$$

²¹ The full expression for the scalar bulk-to-boundary propagator can be written as

$$\mathcal{G}_R(u, q) = (4u)^{\Delta-1/2} (1-u)^{-i\omega/2} (1+u)^{\omega/2} \frac{h(u)}{h(0)},$$

where

$$h(u) = \text{Hl}(2, q^2 + \frac{\Delta^2}{4} - i\Delta_-\omega + \frac{(1+i)\omega}{2} - \frac{i\omega^2}{2}; \frac{\Delta_-}{2} + \frac{(1-i)\omega}{2}, \frac{\Delta_-}{2} + \frac{(1-i)\omega}{2}, 1 - i\omega, \Delta_- - 1; 1 - u),$$

$\Delta_- = \frac{d}{2} - \sqrt{(\frac{d}{2})^2 + m^2 R^2} = d - \Delta$, and Hl is the Heun function [31]. (Compare to footnote 14.) Here we have naively normalized the bulk-to-boundary propagator so that the coefficient of the small- u behavior $(4u)^{\Delta-1/2} = (4u)^{(d-\Delta)/2} = z^{d-\Delta}$ is precisely 1 instead of some more complicated normalization involving regularization of the boundary to some small, finite value z_B of $z \equiv \sqrt{4u}$. As argued by ref. [30], the naive normalization of the bulk-to-boundary propagator can be used when computing n -point functions with $n > 2$.

Substituting the metric factors and the various propagators leads to

$$\begin{aligned} \langle \frac{1}{2} \{ \hat{\Sigma}_\Theta, \hat{\Sigma}_\Theta \} \rangle_{(a-1)} &\simeq \frac{\mathcal{N}_A^2 J^2}{32 g_{\text{SG}}^4} \int \frac{du_1}{u_1^2 f_1} \frac{du_2}{u_2^2 f_2} \mathcal{A}^*(x, u_1) \overleftrightarrow{\partial}_{x^0} i G_{\text{rr}}^{(5)}(x, u_1; y, u_2) \overleftrightarrow{\partial}_{y^0} \mathcal{A}(y, u_2) \\ &+ \{x \leftrightarrow y\}, \end{aligned} \quad (\text{A7})$$

where now

$$\mathcal{A}(x, u) = \int_q \mathcal{G}_R(u; q) \Lambda_L(q - \bar{k}) e^{iq \cdot x}. \quad (\text{A8})$$

The same considerations we have previously made apply: namely we can approximate the action of $\overleftrightarrow{\partial}_{x^0}$ and $\overleftrightarrow{\partial}_{y^0}$ by $-2iE$ factors, substitute the factorized form of the symmetrized propagator, and evaluate the subsequent u integrals,

$$I_{qp} = \int \frac{du}{u^2 f} \mathcal{G}_R(u; q) [\mathcal{G}_R(u; p) - \mathcal{G}_A(u; p)]. \quad (\text{A9})$$

I_{qp} above differs from (5.17) by a factor of $1/u$, but in the near-horizon approximation $u \simeq 1$ and $du/(u^2 f) \simeq d\tau$ it becomes formally identical to (5.19):

$$I_{qp} \simeq ib(q) \left[\frac{b(p)}{q^0 + p^0 + i\epsilon} - \frac{b^*(p)}{q^0 - p^0 + i\epsilon} \right]. \quad (\text{A10})$$

The final result is then the same as (5.25) but with the substitution $\mathcal{N}_A^2 \rightarrow \mathcal{N}_A^2 J^2/4$ in the overall normalization. The conclusion is the same as for the case analyzed in the main text: for late times ($x^0, y^0 \rightarrow \infty$) the integrated charge deposition correlator is exponentially suppressed for $|\mathbf{x} - \mathbf{y}| \gg 1/T$.

Appendix B: Relation of our near-horizon $G_{\text{rr}}^{(5)}$ to ref. [10]

Caron-Huot, Chesler, and Teaney [10] studied correlators of fluctuations of the position $\hat{x}(t, r)$ of a classical string, where r was their coordinate for the 5th dimension, running from $r=1$ at the horizon to $r=\infty$ at the boundary. One of their results was

$$G_{\text{rr}}(t_1, r_1; t_2, r_2) = \int dt'_1 dt'_2 [-G_{\text{ra}}(t_1, r_1; t'_1, r_h)] [-G_{\text{ra}}(t_2, r_2; t'_2, r_h)] G_{\text{rr}}^h(t'_1, t'_2) \quad (\text{B1})$$

for $r_1, r_2 > r_h$, where $r_h = 1 + \epsilon$ with ϵ very small defined a ‘‘stretched’’ horizon and where $G_{\text{rr}}^h(t'_1, t'_2)$ was a type of correlator on that stretched horizon. For our purposes here, we may treat ϵ as infinitesimal. They found that

$$G_{\text{rr}}^h = -\frac{\eta}{\pi} \partial_{v_1} \partial_{v_2} \ln |1 - e^{-2\pi T(v_1 - v_2)}|, \quad (\text{B2})$$

where v is Eddington-Finkelstein time

$$v \equiv t + \frac{1}{\pi T} \int \frac{dr}{fr^2} \quad (\text{B3})$$

evaluated in (B2) at $r_1 = r_2 = r_h$. So (B2) can be rewritten as

$$G_{\text{rr}}^h = -\frac{\eta}{\pi} \partial_{t_1} \partial_{t_2} \ln |1 - e^{-2\pi T(t_1 - t_2)}|. \quad (\text{B4})$$

Their definition of G_{rr} as $\frac{1}{2}\langle\{O(1), O(2)\}\rangle$ for an operator O is $i/2$ times ours, but we will not worry about overall normalization factors in this discussion since the final formulas for G_{rr} also depend how one normalizes the operators of interest to a particular problem.

We will now see that these same equations describe formulas in our paper (up to overall normalization) provided we generalize (B2) to fields with \mathbf{x} dependence,

$$G_{\text{rr}}^{(5)}(x_1, r_1; x_2, r_2) = \int dx'_1 dx'_2 [-G_{\text{ra}}^{(5)}(x_1, r_1; x'_1, r_h)] [-G_{\text{ra}}^{(5)}(x_2, r_2; x'_2, r_h)] G_{\text{rr}}^{\text{h}}(x'_1, x'_2), \quad (\text{B5})$$

and keep (B4) the same.

Fourier transforming (B4) gives

$$G_{\text{rr}}^{\text{h}}(q) \propto \omega \text{cth}(\frac{1}{2}\beta\omega). \quad (\text{B6})$$

The Fourier transform of (B5) is

$$\begin{aligned} G_{\text{rr}}^{(5)}(r_1; r_2, q) &= G_{\text{ra}}^{(5)}(r_1, -q; r_h) G_{\text{ra}}^{(5)}(r_2, q; r_h) G_{\text{rr}}^{\text{h}}(q) \\ &= [G_{\text{R}}^{(5)}(r_h; r_1, q)]^* G_{\text{R}}^{(5)}(r_h; r_2, q) G_{\text{rr}}^{\text{h}}(q), \end{aligned} \quad (\text{B7})$$

given our convention in this paper that G_{R} means G_{ar} .

We can now proceed generally or specialize to the case where r_1 and r_2 are near the horizon (though not as near as r_h). In the latter case, simply plugging in our near-horizon formula (4.17) for $G_{\text{R}}^{(5)}$ and (B6) into (B7) gives

$$G_{\text{rr}}^{(5)} \propto \frac{\text{cth}(\frac{1}{2}\beta\omega)}{\omega} \{e^{i\omega\tau_h} [-e^{i\delta(q)} e^{i\omega\tau_1} + e^{-i\omega\tau_1}]\}^* \{e^{i\omega\tau_h} [-e^{i\delta(q)} e^{i\omega\tau_2} + e^{-i\omega\tau_2}]\}, \quad (\text{B8})$$

which reproduces our near-horizon result (4.22) for $G_{\text{rr}}^{(5)}$. In the more general case, use (4.1) instead of (4.17) to obtain

$$\begin{aligned} G_{\text{rr}}^{(5)} &\propto \omega \text{cth}(\frac{1}{2}\beta\omega) \left\{ \frac{\mathcal{G}_{\text{R}}(u_h; q)}{W_{\text{RA}}(q)} [\mathcal{G}_{\text{R}}(u_1; q) - \mathcal{G}_{\text{A}}(u_1; q)] \right\}^* \left\{ \frac{\mathcal{G}_{\text{R}}(u_h; q)}{W_{\text{RA}}(q)} [\mathcal{G}_{\text{R}}(u_2; q) - \mathcal{G}_{\text{A}}(u_2; q)] \right\} \\ &= \frac{-\omega |\mathcal{G}_{\text{R}}(u_h; q)|^2 \text{cth}(\frac{1}{2}\beta\omega)}{W_{\text{RA}}^*(q) W_{\text{RA}}(q)} [\mathcal{G}_{\text{R}}(u_1; q) - \mathcal{G}_{\text{A}}(u_1; q)] [\mathcal{G}_{\text{R}}(u_2; q) - \mathcal{G}_{\text{A}}(u_2; q)]. \end{aligned} \quad (\text{B9})$$

This reproduces (4.9) with the aid of (4.10) for $\mathcal{G}_{\text{R}}(u_h; q)$ and (4.16).

Appendix C: $T=0$ analysis of $\frac{1}{2}\langle\{j^\mu, j^\nu\}\rangle$

It's useful to see how the formalism used in this paper works in the zero-temperature case. Among other things, it provides a useful double check of the normalization of some of our basic equations.

There is no thermalization and ‘‘charge deposition’’ in vacuum, and so we will study $\frac{1}{2}\langle\{j^\mu(x), j^\nu(y)\}\rangle$ instead of $\frac{1}{2}\langle\{\hat{\Sigma}_\Theta(x), \hat{\Sigma}_\Theta(y)\}\rangle$. At zero temperature, a jet excitation simply propagates forever. The excitation's total current should not change with time, and so it is natural to expect that

$$\begin{aligned} \Delta \left\langle \frac{1}{2} \left\{ \int_{\mathbf{x}} j^\mu(x^0, \mathbf{x}), \int_{\mathbf{y}} j^\nu(y^0, \mathbf{y}) \right\} \right\rangle_{\text{jet}} &\simeq \left\langle \int_{\mathbf{x}} j^\mu(x^0, \mathbf{x}) \right\rangle_{\text{jet}} \left\langle \int_{\mathbf{y}} j^\nu(y^0, \mathbf{y}) \right\rangle_{\text{jet}} \\ &\simeq e_{\text{jet}}^2 \frac{\bar{k}^\mu \bar{k}^\nu}{E^2} \theta(x^0) \theta(y^0) \end{aligned} \quad (\text{C1})$$

at zero temperature. The goal of this appendix is to show that the methods used in this paper indeed reproduce this expected result. Here, $e_{\text{jet}} = 1$ as in the main text. Above, the Δ indicates we subtract (vacuum) fluctuations as in (3.6), analogous to (2.31).

In the following, we will write the zero-temperature metric as

$$ds^2 = \frac{R^2}{4} \left[\frac{1}{\bar{u}} (-dt^2 + d\mathbf{x}^2) + \frac{1}{\bar{u}^2} d\bar{u}^2 \right], \quad (\text{C2})$$

where \bar{u} corresponds to our earlier $u/(2\pi T)^2$ and runs from zero to infinity.

Start from (5.1) and (5.2). As discussed in ref. [3], the low-wavenumber approximation for the observable corresponds to

$$\mathcal{G}_\sigma^{\text{R}\mu}(\bar{u}; Q) \simeq \delta_\sigma^\mu \quad (\text{C3})$$

at zero temperature. In this approximation, (3.14) gives

$$\mathcal{G}_\sigma^{\text{rr}\mu}(\bar{u}; Q) \simeq 0, \quad (\text{C4})$$

and so we can ignore every diagram in fig. 13 except (a-1). Combining (5.1) and (5.2) using (C3) gives

$$\begin{aligned} \Delta \langle \frac{1}{2} \{j^\mu, j^\nu\} \rangle &\simeq \frac{\mathcal{N}_A^2}{4g_{\text{SG}}^4} \int \frac{d\bar{u}_1}{\bar{u}_1} \frac{d\bar{u}_2}{\bar{u}_2} \mathcal{A}^*(x, \bar{u}_1) \overleftrightarrow{\partial}_{x^\mu} iG_{\text{rr}\perp}^{(5)}(x, \bar{u}_1; y, \bar{u}_2) \overleftrightarrow{\partial}_{y^\nu} \mathcal{A}(y, \bar{u}_2) \\ &+ \{x \leftrightarrow y\}. \end{aligned} \quad (\text{C5})$$

Note that the zero-temperature formula for $\frac{1}{2} \langle \{j^0, j^0\} \rangle$ happens to have exactly the same form as the finite-temperature formula (5.9) for $\frac{1}{2} \langle \{\hat{\Sigma}_\Theta, \hat{\Sigma}_\Theta\} \rangle$ (noting that $f \rightarrow 1$ at zero temperature). Following the same line of argument that led to (5.14) then gives the analogous zero-temperature formula

$$\begin{aligned} \Delta \langle \frac{1}{2} \{j^\mu, j^\nu\} \rangle &\simeq \\ &- 2\bar{k}^\mu \bar{k}^\nu \frac{\mathcal{N}_A^2}{g_{\text{SG}}^4} \text{Re} \int_p \int \frac{d\bar{u}_1}{\bar{u}_1} \frac{d\bar{u}_2}{\bar{u}_2} \mathcal{A}^*(x, \bar{u}_1) e^{ip \cdot x} iG_{\text{rr}\perp}^{(5)}(\bar{u}_1; \bar{u}_2, -p) e^{-ip \cdot y} \mathcal{A}(y, \bar{u}_2). \end{aligned} \quad (\text{C6})$$

It's helpful at this point to have the explicit formulas for the transverse-polarized bulk-to-boundary propagators in 4-momentum space, which are

$$\mathcal{G}(\bar{u}; q) = \sqrt{4\bar{u}q^2} K_1(\sqrt{4\bar{u}q^2}), \quad (\text{C7})$$

where K_n is the modified Bessel function of the second kind. q^0 in this formula means $q^0 + i\epsilon$ for the retarded propagator and $q^0 - i\epsilon$ for the advanced propagator. The Wronskian (4.7), which is most easily evaluated in the $\bar{u} \rightarrow 0$ limit, is then

$$W_{\text{RA}}(q) = i\pi R q^2 \text{sign}(q^0). \quad (\text{C8})$$

Note also that the zero-temperature ($\beta \rightarrow \infty$) limit of the fluctuation-dissipation relation (3.3) is

$$iG_{rr}(q) = \text{sign}(q^0) [iG_{\text{R}}(q) - iG_{\text{A}}(q)]. \quad (\text{C9})$$

Comparing (C8) to the finite-temperature formula (4.16), the upshot is that the analysis of $\langle \frac{1}{2}\{j^\mu, j^\nu\} \rangle$ at zero temperature goes through just as the finite-temperature derivation of (5.15) for $\langle \frac{1}{2}\{\hat{\Sigma}_\Theta^\mu, \hat{\Sigma}_\Theta^\nu\} \rangle$ but with the replacement

$$\frac{\text{cth}(\frac{1}{2}\beta p^0)}{p^0 |b(p)|^2} \rightarrow -\frac{1}{\pi p^2}, \quad (\text{C10})$$

to give

$$\Delta \langle \frac{1}{2}\{j^\mu, j^\nu\} \rangle \simeq -2\bar{k}^\mu \bar{k}^\nu \frac{\mathcal{N}_A^2}{g_{\text{SG}}^2} \text{Re} \int_p \frac{1}{\pi p^2} \mathcal{J}^*(p, x) \mathcal{J}(p, y), \quad (\text{C11})$$

with \mathcal{J} defined as before in (5.16). Using (C7), the desired u -integral (5.17) of \mathcal{J} is given explicitly by

$$\begin{aligned} I_{qp} &= 4\pi i \theta(-p^2) \sqrt{-p^2 q^2} \int_0^\infty d\bar{u} K_1(\sqrt{4\bar{u}q^2}) J_1(\sqrt{-4\bar{u}p^2}) \\ &= 2\pi i \frac{p^2}{p^2 - q^2} \theta(-p^2) \end{aligned} \quad (\text{C12})$$

with q^0 interpreted as $q^0 + i\epsilon$. Substitution into (5.16) gives

$$\mathcal{J}(p, x) = -2\pi i p^2 \theta(-p^2) \int_q \tilde{\Lambda}_L(q - \bar{k}) \frac{e^{i(q-p)\cdot x}}{q^2 - p^2} \quad (\text{C13})$$

as the zero-temperature analog of (5.20), but note that we have not made anything analogous to the ‘‘near-horizon’’ approximation in the zero-temperature analysis.

Since our sanity check (C1) of results and normalizations in this appendix involves integrating over 3-position, it’s convenient at this point to integrate (C13) over \mathbf{x} to get

$$\int_{\mathbf{x}} \mathcal{J} = ip^2 \theta(-p^2) \int dq^0 \frac{e^{-i(q^0 - p^0)x^0}}{(q^0 + i\epsilon)^2 - (p^0)^2} \tilde{\Lambda}_L(q^0 - E, \mathbf{p}^\perp, p^3 - E). \quad (\text{C14})$$

Following similar approximations as from (5.20) to (5.23), pick up only the explicit poles in (C14) and then throw away highly-oscillatory terms in the result. This yields

$$\begin{aligned} \int_{\mathbf{x}} \mathcal{J} &\simeq \frac{\pi p^2}{p^0} \theta(-p^2) \theta(x^0) \tilde{\Lambda}_L(p - \bar{k}) \\ &\simeq 4\pi p_+ \theta(-p_+) \theta(x^0) \tilde{\Lambda}_L(p - \bar{k}). \end{aligned} \quad (\text{C15})$$

Using this expression in (C11) gives

$$\begin{aligned} \Delta \langle \frac{1}{2}\{\int_{\mathbf{x}} j^\mu, \int_{\mathbf{y}} j^\nu\} \rangle &\simeq -32\pi \bar{k}^\mu \bar{k}^\nu \theta(x^0) \theta(y^0) \frac{\mathcal{N}_A^2}{g_{\text{SG}}^2} \int_p \theta(-p_+) \frac{(p_+)^2}{p^2} \left| \tilde{\Lambda}_L(p - \bar{k}) \right|^2 \\ &\simeq \mathcal{Q} \frac{\bar{k}^\mu \bar{k}^\nu}{E^2} \theta(x^0) \theta(y^0), \end{aligned} \quad (\text{C16})$$

where

$$\mathcal{Q} \simeq 8\pi E \frac{\mathcal{N}_A^2}{g_{\text{SG}}^2} \int_q \theta(-q_+) |q_+| \left| \tilde{\Lambda}_L(q) \right|^2. \quad (\text{C17})$$

This formula for \mathcal{Q} is equivalent to that found in ref. [3] for the average charge created by our source operator. Dividing both sides of (C16) by \mathcal{Q} and invoking (2.19) finally gives us (C1), as expected.

-
- [1] D. T. Son and A. O. Starinets, “Viscosity, Black Holes, and Quantum Field Theory,” *Ann. Rev. Nucl. Part. Sci.* **57**, 95 (2007) [arXiv:0704.0240].
 - [2] R. Baier, P. Romatschke, D. T. Son, A. O. Starinets and M. A. Stephanov, “Relativistic viscous hydrodynamics, conformal invariance, and holography,” *JHEP* **0804**, 100 (2008) [arXiv:0712.2451].
 - [3] P. Arnold, D. Vaman, “Jet quenching in hot strongly coupled gauge theories revisited: 3-point correlators with gauge-gravity duality,” *JHEP* **1010**, 099 (2010) [arXiv:1008.4023].
 - [4] P. Arnold, D. Vaman, “Jet quenching in hot strongly coupled gauge theories simplified,” *JHEP* **1104**, 027 (2011) [arXiv:1101.2689].
 - [5] P. Arnold, D. Vaman, “Some new results for ‘jet’ stopping in AdS/CFT,” arXiv:1106.1680, an abridged version to appear in *J. Phys. G*.
 - [6] P. Arnold, D. Vaman, C. Wu, W. Xiao, “Second order hydrodynamic coefficients from 3-point stress tensor correlators via AdS/CFT,” *JHEP* **1110**, 033 (2011) [arXiv:1105.4645].
 - [7] O. Saremi, K. A. Sohrabi, “Causal three-point functions and nonlinear second-order hydrodynamic coefficients in AdS/CFT,” arXiv:1105.4870.
 - [8] Y. Hatta, T. Ueda, “Soft photon anomaly and gauge/string duality,” *Nucl. Phys.* **B837**, 22-39 (2010) [arXiv:1002.3452].
 - [9] L. Fidkowski, V. Hubeny, M. Kleban and S. Shenker, “The black hole singularity in AdS/CFT,” *JHEP* **0402**, 014 (2004) [arXiv:hep-th/0306170].
 - [10] S. Caron-Huot, P. M. Chesler, D. Teaney, “Fluctuation, dissipation, and thermalization in non-equilibrium AdS₅ black hole geometries,” [arXiv:1102.1073].
 - [11] P. M. Chesler, K. Jensen and A. Karch, “Jets in strongly-coupled $\mathcal{N}=4$ super Yang-Mills theory,” *Phys. Rev. D* **79**, 025021 (2009) [arXiv:0804.3110].
 - [12] G. Policastro, D. T. Son and A. O. Starinets, “From AdS/CFT correspondence to hydrodynamics,” *JHEP* **0209**, 043 (2002) [arXiv:hep-th/0205052].
 - [13] R. Kubo, “The fluctuation-dissipation theorem,” *Rep. Prog. Phys.* **29**, 244 (1966).
 - [14] E. Wang and U. W. Heinz, “A generalized fluctuation-dissipation theorem for nonlinear response functions,” *Phys. Rev. D* **66**, 025008 (2002) [arXiv:hep-th/9809016].
 - [15] D. T. Son, D. Teaney, “Thermal Noise and Stochastic Strings in AdS/CFT,” *JHEP* **0907**, 021 (2009) [arXiv:0901.2338].
 - [16] S. Caron-Huot, O. Saremi, “Hydrodynamic Long-Time tails From Anti de Sitter Space,” *JHEP* **1011**, 013 (2010) [arXiv:0909.4525].
 - [17] G. W. Gibbons, M. J. Perry, *Phys. Rev. Lett.* **36**, 985 (1976).
 - [18] C. P. Herzog and D. T. Son, “Schwinger-Keldysh propagators from AdS/CFT correspondence,” *JHEP* **0303**, 046 (2003) [arXiv:hep-th/0212072].
 - [19] A. Kamenev and A. Levchenko, “Keldysh technique and non-linear σ -model: basic principles and applications,” *Adv. in Phys.* **58** (2009) 197. [arXiv:0901.3586].
 - [20] P. M. Chaikin and T. C. Lubensky, *Principles of Condensed Matter Physics* (Cambridge University Press, 1995).
 - [21] M. J. G. Veltman, “Unitarity and causality in a renormalizable field theory with unstable

- particles,” *Physica* **29**, 186 (1963); G. ’t Hooft and M. J. G. Veltman, “Diagrammar,” NATO Adv. Study Inst. Ser. B Phys. **4**, 177 (1974).
- [22] F. Gelis, “A New approach for the vertical part of the contour in thermal field theories,” *Phys. Lett.* **B455**, 205-212 (1999) [hep-ph/9901263]; “The Effect of the vertical part of the path on the real time Feynman rules in finite temperature field theory,” *Z. Phys.* **C70**, 321-331 (1996) [hep-ph/9412347].
- [23] E. Barnes, D. Vaman, C. Wu, P. Arnold, “Real-time finite-temperature correlators from AdS/CFT,” *Phys. Rev.* **D82**, 025019 (2010). [arXiv:1004.1179].
- [24] K. Skenderis and B. C. van Rees, “Real-time gauge/gravity duality,” *Phys. Rev. Lett.* **101**, 081601 (2008) [arXiv:0805.0150].
- [25] K. Skenderis and B. C. van Rees, “Real-time gauge/gravity duality: Prescription, Renormalization and Examples,” *JHEP* **0905**, 085 (2009) [arXiv:0812.2909].
- [26] L. J. Romans, “Gauged $N=4$ Supergravities In Five-Dimensions And Their Magnetovac Backgrounds,” *Nucl. Phys. B* **267**, 433 (1986).
- [27] H. Lu, C. N. Pope and T. A. Tran, “Five-dimensional $N=4$, $SU(2)\times U(1)$ gauged supergravity from type IIB,” *Phys. Lett. B* **475**, 261 (2000) [arXiv:hep-th/9909203].
- [28] G. Policastro, D. T. Son, A. O. Starinets, “From AdS/CFT correspondence to hydrodynamics, II. Sound waves,” *JHEP* **0212**, 054 (2002). [hep-th/0210220].
- [29] E. Witten, “Anti-de Sitter space and holography,” *Adv. Theor. Math. Phys.* **2**, 253 (1998) [arXiv:hep-th/9802150].
- [30] D. Z. Freedman, S. D. Mathur, A. Matusis and L. Rastelli, “Correlation functions in the $CFT(d)/AdS(d+1)$ correspondence,” *Nucl. Phys. B* **546**, 96 (1999) [arXiv:hep-th/9804058].
- [31] R. S. Maier, “The 192 Solutions of the Heun Equation”, *Math. Computation* **76**, 811 (2007) [arXiv:math/0408317].